AGU PUBLICATIONS

Water Resources Research

RESEARCH ARTICLE
10.1002/2016WR019949

Special Section:
Emergent Aquatic Carbon-nutrient Dynamics as Products of Hydrological, Biogeochemical, and Ecological Interactions

Covariation in patterns of turbulence-driven hyporheic flow and denitrification enhances reach-scale nitrogen removal

Angang Li[1], Antoine F. Aubeneau[2], Diogo Bolster[3], Jennifer L. Tank[4], and Aaron I. Packman[1]

[1]Civil and Environmental Engineering, Northwestern University, Evanston, Illinois, USA, [2]Lyles School of Civil Engineering, Purdue University, West Lafayette, Indiana, USA, [3]Civil and Environmental Engineering and Earth Sciences, University of Notre Dame, Notre Dame, Indiana, USA, [4]Department of Biological Sciences, University of Notre Dame, Notre Dame, Indiana, USA

Key Points:
- We develop a stochastic particle-tracking model to simulate flow-denitrification interactions across the stream-hyporheic continuum
- Nutrient uptake from the stream is controlled primarily by flushing of highly bioactive regions near the sediment-water interface
- Covariation in patterns of hyporheic flow and denitrification cause reach-scale nitrogen removal to increase with subsurface heterogeneity

Supporting Information:
- Supporting Information S1
- Movie S1
- Movie S2
- Movie S3
- Movie S4

Correspondence to:
A. Packman,
a-packman@northwestern.edu

Citation:
Li, A., A. F. Aubeneau, D. Bolster, J. L. Tank, and A. I. Packman (2017), Covariation in patterns of turbulence-driven hyporheic flow and denitrification enhances reach-scale nitrogen removal, *Water Resour. Res.*, *53*, doi:10.1002/2016WR019949.

Received 15 OCT 2016
Accepted 13 JUL 2017
Accepted article online 15 JUL 2017

Abstract Coinjections of conservative tracers and nutrients are commonly used to assess travel time distributions and nutrient removal in streams. However, in-stream tracer data often lack information on long-term hyporheic storage, and removal rate coefficients are often assumed to be uniform despite plentiful evidence that microbially mediated transformations, such as denitrification, exhibit strong spatial variability in the hyporheic zone. We used process-based particle-tracking simulations to explore the coupled effects of spatial patterns in hyporheic flow and denitrification on reach-scale nitrogen removal. We simulated whole-stream nitrogen dynamics with exponential, layered, and uniform profiles of hyporheic denitrification. We also simulated nitrogen dynamics in Little Rabbit Creek, an agricultural headwater stream in the Kalamazoo River Basin (Michigan, USA) where vertical profiles of hyporheic denitrification were measured in situ. Covariation between pore water velocity and mixing causes rapid exchange in the near-surface bioactive region and substantially prolonged exchange in the deeper hyporheic. Patterns of hyporheic denitrification covary with patterns of hyporheic flow. This covariation directly controls tailing of in-stream breakthrough curves and hence reach-scale nutrient removal. Enhanced denitrification near the sediment-water interface strongly tempers breakthrough curve tails at time scales associated with flushing of the near-surface region, while more spatially uniform denitrification causes weaker tempering over a wider range of hyporheic exchange time scales. At the reach scale, overall nitrogen removal increases with heterogeneity of hyporheic denitrification, indicating that covariation between flow and denitrification—particularly the rapid flushing of highly bioactive regions near the sediment-water interface—controls whole-stream transformation rates.

1. Introduction

Excess nutrients in rivers adversely affect aquatic environments, triggering hypoxia, and creating dead zones in numerous coastal systems [*Diaz and Rosenberg*, 2008; *Rabalais et al.*, 2009; *Conley et al.*, 2011; *Chislock et al.*, 2013]. Given the significant role of rivers in facilitating nutrient removal during transport from terrestrial sources to oceans [*Peterson et al.*, 2001; *Mulholland et al.*, 2008; *Seitzinger*, 2008; *Boano et al.*, 2014], there is a pressing need for improved understanding of nutrient dynamics in rivers. Hyporheic exchange between the stream and underlying pore water favors retention and microbially mediated transformation of nutrients [*Triska et al.*, 1989; *McClain et al.*, 2003; *Argerich et al.*, 2008; *Merill and Tonjes*, 2014]. Hyporheic exchange is driven by flow interactions with diverse topographic features [*Thibodeaux and Boyle*, 1987; *Boudreau*, 2000; *Nepf*, 2004; *O'Connor and Harvey*, 2008; *Buffington and Tonina*, 2009; *Sawyer et al.*, 2011] and produces wide distributions of residence times [*Gooseff et al.*, 2007; *Worman et al.*, 2007; *Stonedahl et al.*, 2010; *Aubeneau et al.*, 2014, 2015b]. In sand and gravel bed streams and rivers, downstream velocity and vertical mixing are highest in the stream and decrease with depth in sediment [*Packman et al.*, 2004; *Chandler et al.*, 2016]. These velocity and mixing profiles result in rapid flushing of shallow sediments, and slow transport and longer-term retention of nutrients in deeper sediments [*Savant et al.*, 1987; *Worman et al.*, 2002; *Zaramella et al.*, 2003; *Zarnetske et al.*, 2008; *Marzadri et al.*, 2010; *Fabian et al.*, 2011; *Briggs et al.*, 2014; *Aubeneau et al.*, 2015a]. The hyporheic zone exhibits sharp chemical gradients, and high microbial activity, predominantly in biofilms [*Costerton and Lappin-Scott*, 1995; *Craft et al.*, 2002; *Battin et al.*, 2008,

2016]. Because microbial activity is directly controlled by delivery and retention of nutrients [*Seitzinger et al*., 2006; *Inwood et al*., 2007; *Battin et al*., 2008; *Zarnetske et al*., 2011a], microbial activity often covaries with hyporheic flow and exhibits extensive vertical variability [*Lovley and Chapelle*, 1995; *Seitzinger et al*., 2006; *Inwood et al*., 2007; *Harvey et al*., 2013]. Denitrification, for example, is often observed to be highest near the sediment-water interface (SWI) and decreases with depth in sand and gravel streambeds [*Garcia-Ruiz et al*., 1998a; *Inwood et al*., 2007; *Harvey et al*., 2013]. Further, high denitrification rates often occur in shallow sediments despite bulk oxygenated conditions owing to hypoxic and anoxic microsites within sediments and biofilms [*Arango et al*., 2007; *Arnon et al*., 2007; *O'Connor and Hondzo*, 2007, 2008; *Harvey et al*., 2013; *Briggs et al*., 2015]. At the reach scale, nutrient dynamics depend on the coupling between microbially mediated transformations along hyporheic flow paths and residence times along these paths [*Zarnetske et al*., 2011b; *Harvey et al*., 2013; *Briggs et al*., 2014]. Improved assessment of reach-scale nutrient dynamics therefore requires better approaches to upscale the coupled effects of hyporheic flow and biogeochemical transformation.

Reach-scale nutrient dynamics are often estimated by coinjecting conservative and reactive tracers into the stream, and interpreting downstream breakthrough curves (BTCs) with 1-D models [*Newbold et al*., 1982; *Bencala and Walters*, 1983; *Harvey and Wagner*, 2000; *Marion and Zaramella*, 2005; *Covino et al*., 2010; *O'Connor et al*., 2010]. Commonly used models include the spiraling model [*Webster and Patten*, 1979; *Newbold et al*., 1981; *Covino et al*., 2010] and transient storage model (TSM) [*Bencala and Walters*, 1983; *Runkel*, 1998; *Bencala et al*., 2011]. These reach-scale models typically estimate effective reach-scale coefficients by fitting in-stream BTCs using one of these models, assuming that the hyporheic zone is homogeneous. Assumptions of homogeneity are based on a lack of information on spatial distributions within the hyporheic zone. Hyporheic reactions are therefore represented by a spatially invariant reaction rate constant [*Boano et al*., 2014], despite the fact that hyporheic flow and microbially mediated transformations exhibit pronounced vertical variability [*Garcia-Ruiz et al*., 1998a; *Inwood et al*., 2007; *Harvey et al*., 2013]. Further, fitting of whole-stream transport and reaction coefficients generally assumes that hyporheic flow and transformation rates are independent, which leads to uncertainty in estimating both hyporheic transformation rates and the effects of changing flow conditions on reach-scale dynamics [*González-Pinzón et al*., 2013; *Ward et al*., 2014; *Harman et al*., 2016; *Schmadel et al*., 2016]. An improved understanding of the complex dynamics requires a reach-scale model that explicitly simulates covariation of flow and transformation processes within the hyporheic zone. While prior studies have simulated coupled flow and biogeochemical processes in advective hyporheic exchange induced by topographic features such as dunes and bars, no studies have examined the more basic coupling associated with fundamental patterns of vertical turbulent mixing into sediments [*González-Pinzón et al*., 2013; *Marzadri et al*., 2014; *Bellin et al*., 2015].

The objective of this study was to investigate how coupling between vertical covariation of hyporheic flow and microbially mediated transformation enhances reach-scale nutrient removal in sand and gravel bed rivers. We hypothesized that reach-scale nitrogen removal increases with subsurface heterogeneity for the most common case where the denitrification rate decreases monotonically with depth in the hyporheic zone. Here we test this hypothesis with a particle-tracking model that explicitly represents vertical covariation of flow and denitrification throughout the stream-subsurface continuum. We simulate conservative tracer dynamics to demonstrate how vertical covariation in hyporheic velocity and mixing controls residence time distributions. We then evaluate nitrogen dynamics with several different patterns of hyporheic denitrification to quantify the effects of covarying flow and denitrification on reach-scale nitrogen removal. Finally, we analyze data from Little Rabbit Creek, an agricultural headwater stream in the Kalamazoo River Basin (Michigan, USA), to demonstrate the effects of flow-denitrification coupling on reach-scale nitrogen removal in a stream enriched with nitrate.

2. Methods

2.1. Particle-Tracking Framework

Reach-scale simulations were performed with a stochastic particle-tracking model framework that uses a discrete representation of tracer mass. The model tracks the ensemble behavior of a statistically large number of discretized mass elements ("virtual particles") subject to spatial distributions of flow and hyporheic denitrification. Downstream mass transport in rivers is classically described by a longitudinal advection-dispersion equation, which assumes steady, uniform, and fully developed turbulent flow. However, a two-

dimensional representation is needed to capture the effects of spatial covariation of flow and denitrification in the hyporheic zone. Assuming negligible transverse variability, zero vertical velocity, fully developed turbulent flow, and negligible longitudinal turbulent diffusion relative to dispersion [*Fischer*, 1979], we can write a two dimensional advection-dispersion equation that spans the downstream (x) and vertical (y) directions [*Fischer et al*., 1979]:

$$\frac{\partial C}{\partial t}+u_x(y)\frac{\partial C}{\partial x}=\frac{\partial}{\partial y}\left(D_y(y)\frac{\partial C}{\partial y}\right) \tag{1}$$

where $C(x,y,t)$ is concentration, t is time, $u_x(y)$ is depth-varying downstream velocity, x is downstream position, y is vertical position, and $D_y(y)$ is depth-varying vertical turbulent diffusion coefficient in the water column and the vertical dispersion coefficient in the hyporheic zone. Note that this model inherently captures the effects of longitudinal dispersion, as longitudinal dispersion results from the integration of equation (1) over the depth of the stream [*Taylor*, 1954; *Elder*, 1959; *Fischer*, 1979]. Also note that here we assess flow and transport both in the stream and subsurface, thereby extending prior theoretical and modeling studies of longitudinal dispersion and travel time distributions in rivers to include the full stream-hyporheic flow continuum. The following 2-D Langevin equation, which tracks the position of particle representing the solute of interest, provides a discrete Lagrangian analogue to the above advection-dispersion equation [*Kinzelbach*, 1988; *Delay et al*., 2005]:

$$x(t+\Delta t)=x(t)+u_x\Delta t \tag{2}$$

$$y(t+\Delta t)=y(t)+\frac{\partial D_y}{\partial y}\Delta t+\xi\sqrt{2D_y\Delta t}$$

where Δt is a time step and ξ is a normally distributed random variable with zero mean and unit variance. Equation (2) is useful for assessing ensemble reach-scale transport using particle-tracking methods, which avoid spatial discretization errors (such as numerical dispersion) that occur when simulating equation (1) [*Kitanidis*, 1994; *Salamon et al*., 2006; *Robinson et al*., 2010]. Specifying velocity and dispersion at all depths including in the surface and subsurface allows us to evaluate the complete velocity and mixing distributions for the entire stream-subsurface continuum. This approach enables simulation of in-stream and hyporheic transport in a single and consistent framework.

We represent hyporheic denitrification as a first-order process, where the rate constant varies with depth. Within the stochastic framework of equation (2), this can be applied by calculating the probability (p) that discretized mass is removed due to denitrification during a given time step [*Prickett et al*., 1981]:

$$p=1-e^{-k\Delta t}\approx k\Delta t \tag{3}$$

where $k(y)$ is the first-order denitrification rate constant. The time step in the simulations is set sufficiently small ($\Delta t = 1$ s) to ensure that the Taylor expansion approximation in (3) holds.

2.2. Simulation Conditions

We performed simulations using depth-varying denitrification rate constants, $k(y)$, velocity distributions, $u_x(y)$, and mixing distributions, $D_y(y)$, to assess the effects of covariances in these distributions on integrated reach-scale transformation rates. We introduced discretized tracer mass, uniformly distributed, into the water column at $x = 0$ to simulate pulse injections in the field [*Covino et al*., 2010]. The propagation of tracer mass is analyzed by tracking the location of each discrete tracer mass element by equation (2), and accounting for mass removal by reaction with equation (3).

As a baseline case, we simulate flow and transport for flow depth, velocity and dispersion profiles representative of a small gravel bed stream. Stream morphology, flow, and denitrification parameters are summarized in supporting information Table S1. We represent the time-averaged turbulent free-surface flow velocity with a classical log-law profile [*Beavers and Joseph*, 1967; *Mendoza and Zhou*, 1992; *Manes et al*., 2011]:

$$u_x=\frac{u_*}{\kappa}\ln\left(\frac{y+y_0}{y_0}\right)+U_s \tag{4}$$

where u_* is shear velocity, κ is von Karman constant, y_0 is a characteristic length, and U_s is the slip velocity at the SWI due to penetration of turbulence from the stream. The characteristic length is an empirical length

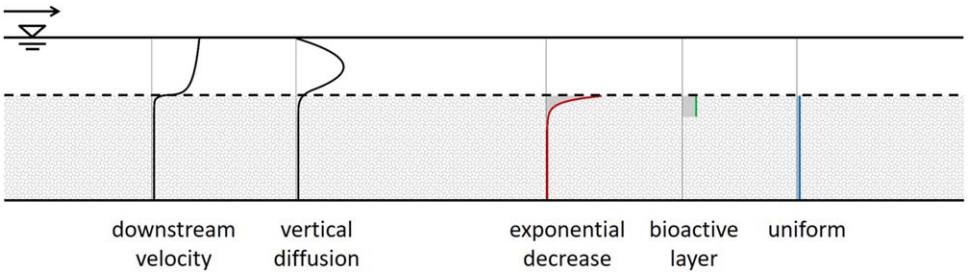

Figure 1. Schematic of stream and subsurface conditions used to simulate reach-scale conservative transport and nitrogen dynamics. Turbulent stream flow is coupled with hyporheic pore water flow in the permeable sediment bed. The dashed line represents the sediment-water interface. The velocity profile is logarithmic in the water column and transitions exponentially at the sediment-water interface to a constant underflow velocity deep in the bed. The underflow velocity is based on applying Darcy's law with the channel slope. Hyporheic denitrification was simulated using exponential, layered, and uniform distributions of first-order reaction rate coefficients, with identical mean (depth-averaged) reaction rates.

scale that characterizes the effect of porous bed on in-stream velocity. Shear velocity is taken as $u_* = \sqrt{gHS}$, where g is gravitational acceleration, H is the mean river depth, and S is the free surface slope [*Fischer et al*., 1979]. The velocity distribution in the subsurface is represented as an exponential transition between the logarithmic velocity profile (4) and Darcy flow in the deep subsurface (Figure 1) [*Nagaoka and Ohgaki*, 1990; *Zhou and Mendoza*, 1993]:

$$u_x = U_D + (U_s - U_D)\ \exp(My) \tag{5}$$

where U_D is the seepage velocity for the underlying pore water flow (underflow) and M is a dimensional constant representing the rate of velocity decay in the near-surface region. This model is applicable for a wide range of sediments, including gravel and sand [*Nagaoka and Ohgaki*, 1990; *Zhou and Mendoza*, 1993]. The velocity decay constant M is dependent on the pressure gradient and the structure of the porous media, particularly the sediment grain size [*Beavers and Joseph*, 1967; *Nagaoka and Ohgaki*, 1990]. The underflow is obtained by applying Darcy's law based on the channel slope $U_D = \frac{KS}{n}$, where K is the hydraulic conductivity and n is the porosity of the hyporheic sediments [*Elliott and Brooks*, 1997b, 1997a].

We assume slope $S = 1 \times 10^{-4}$, stream depth $H = 0.5$ m, and median grain diameter $D_{50} = 1$ cm as representative for gravel bed streams (supporting information Table S1). We assign the sediment depth to be 1 m, which is sufficiently large to avoid restricting the exponential transition profile, and yields a substantial region of underflow beneath the exponential region. This depth is also consistent with the most commonly reported ranges of hyporheic zone depth in gravel bed rivers with high denitrification rates [*Fellows et al*., 2001; *Fischer et al*., 2005; *Gooseff et al*., 2006; *Ward*, 2016]. In order to relate water column, interfacial, and hyporheic flow, we base estimates of y_0, M, and K on the sediment grain diameter. The characteristic length in the overlying turbulent velocity profile (4) is obtained from the empirical relationship $y_0 = D_{50}\ \exp\left[\kappa\left(\frac{U_s}{u_*} - 9.09\right)\right]$ [*Zagni and Smith*, 1976; *Mendoza and Zhou*, 1992]. Hydraulic conductivity is estimated as $K = 100 D_{50}^2$ [*Bear*, 1972; *Uma et al*., 1989]. Finally, we assign a slip velocity of $U_s = 0.1$ m/s and decay constant $M = 200\ \mathrm{m}^{-1}$ based on reported experimental values representative of gravel beds [*Nagaoka and Ohgaki*, 1990; *Habel et al*., 2002]. The resulting mean water column velocity $<u_x> = 0.38$ m/s and underflow velocity $U_D = 1 \times 10^{-6}$ m/s.

The distribution of vertical mixing is also described as a smooth transition between the turbulent free-surface flow and Darcy flow in porous media. The turbulent diffusion coefficient in the water column follows conventional theory for free-surface flow [*Fischer et al*., 1979]:

$$D_y = u_*^2 \left(1 - \frac{y}{H}\right) \frac{dy}{du_x} \tag{6}$$

In the deep subsurface, where Darcy's law applies, the vertical dispersion coefficient is estimated as $D_y = D_{50}\ u_x$ [*Bear*, 1972]. In the interfacial region, we interpolated the vertical mixing coefficient between values for the overlying turbulent free-surface flow and the underlying Darcy pore water flow using piecewise cubic Hermite interpolation. We considered enhanced interfacial transport to a depth of 10 grain diameters ($y = -0.1$ m), based on experimental observations for gravel streambeds [*Packman et al*., 2004].

The vertical mixing coefficient averaged $D_y = 8 \times 10^{-4}$ m^2/s in the water column and 1×10^{-8} m^2/s in the deep subsurface. Note the tremendous disparities between in-stream and subsurface transport: the underflow velocity is ~5 orders of magnitude lower than the mean in-stream velocity, while the vertical pore water dispersion coefficient is ~5 orders of magnitude lower than the in-stream turbulent diffusion coefficient. These high disparities between in-stream and subsurface transport are characteristic of hyporheic exchange [*Ren and Packman*, 2002; *Worman et al*., 2002; *Packman and MacKay*, 2003; *Packman et al*., 2004; *Rehg et al*., 2005; *Higashino et al*., 2009; *Stonedahl et al*., 2010, 2012; *Camarena et al*., 2016].

We simulate hyporheic denitrification using three distinct first-order rate profiles that are commonly found for hyporheic denitrification: exponential, layered, and uniform distributions (Figure 1). In some streams, hyporheic denitrification has been observed to be greatest just at the SWI and to decline approximately exponentially with depth, with denitrification in the deeper sediment limited by availability of nutrients and organic carbon [*Garcia-Ruiz et al*., 1998b; *Inwood et al*., 2007; *Lansdown et al*., 2012; *Harvey et al*., 2013]. For this exponential case, we set the maximum denitrification rate constant to be 1×10^{-3} s^{-1} and exponential decay rate to be 20 m^{-1} based on first-order denitrification profiles reported in the literature [*Sheibley et al*., 2003; *Harvey et al*., 2013; *Sawyer*, 2015]. In other systems, denitrification has been observed to be confined within the top 0.05–0.25 m of the streambed, and to be approximately constant over this depth [*Christensen et al*., 1990; *Lefebvre et al*., 2004; *Arango et al*., 2007; *Herrman et al*., 2008; *Stelzer et al*., 2011; *Roley et al*., 2012]. We simulate this case with denitrification limited to a bioactive layer 0.2 m deep and occurring with a rate constant of 2.5×10^{-4} s^{-1}. Finally, we simulate a uniform denitrification profile to match the assumptions of the most commonly used reach-scale models, such as the TSM, which represent hyporheic denitrification with a single, spatially invariant rate coefficient based on the assumption that the hyporheic zone is well mixed [*Boano et al*., 2014]. The denitrification rate constant in the uniform case is 5×10^{-5} s^{-1}, matching the depth-averaged hyporheic denitrification rate for both the exponential and layered cases. All simulation parameters are summarized in supporting information Table S1. The use of identical depth-averaged denitrification rates, stream morphology, and flow parameters in all three cases supports direct evaluation of the effects of spatial heterogeneity in hyporheic denitrification on reach-scale nitrogen dynamics.

3. Results

3.1. Conservative Tracer Dynamics

Hyporheic exchange induces long-term retention that is reflected in the pronounced tailing observed in a sample snapshot (Figure 2) and the full evolution (supporting information Movie S1) for conservative tracer transport in the coupled surface-subsurface domain. The results are presented as 2-D spatial distributions of concentration, 1-D (depth-averaged) spatial snapshots, and BTCs. Tracer mass is initially uniformly

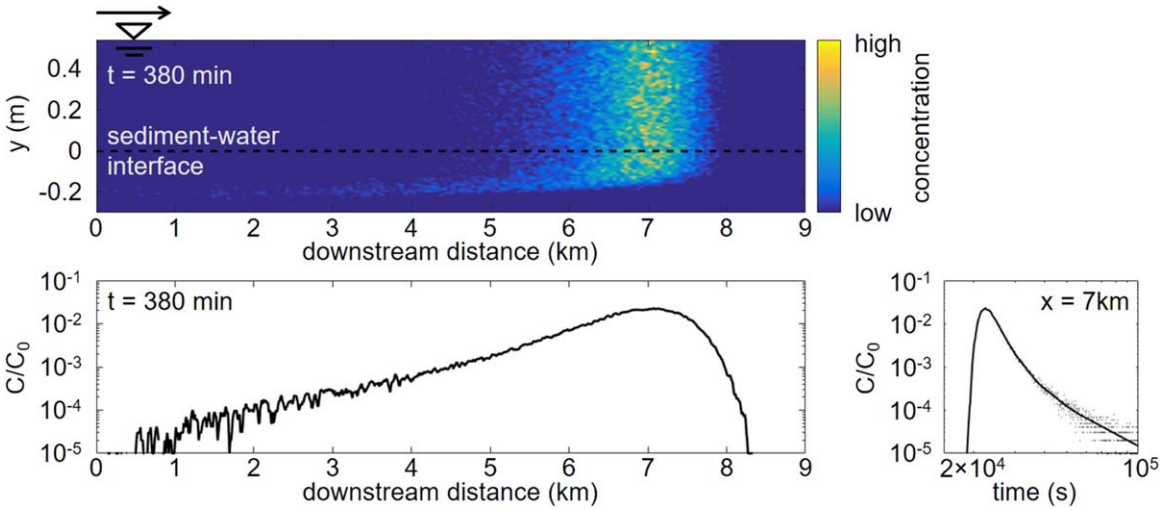

Figure 2. Concentration snapshots and breakthrough curves for conservative tracer transport. (top) Heat map of tracer concentrations across the entire 2-D domain 380 min after pulse injection into the water column. The sediment-water interface is indicated by the dashed line at $y = 0$. (bottom left) Corresponding spatial snapshot of in-stream concentration. (bottom right) In-stream breakthrough curve 7 km downstream of injection location.

distributed in the water column but penetrates into the sediment during downstream transport, leading to strong disparities in transport between the surface and subsurface domains. Fast vertical mixing in the water column and across the SWI results in a nearly uniform tracer concentration distribution through the water column and the SWI at all times. Rapid mixing also causes the tracer concentration peak to propagate at a velocity (0.31 m/s) less than the mean in-stream velocity (0.38 m/s), because tracer mass is subject to slower velocities after crossing the SWI. Tracer that exchanges with the deeper hyporheic zone is subject to very strong delays and thus travels downstream much more slowly. This causes substantial anomalous dispersion in downstream transport, which is reflected in power law tails in both spatial snapshots and BTCs [*Van Kampen*, 1992; *Aquino et al*., 2015, 2017]. The spatial snapshot shows a very steep leading edge corresponding to the peak of the in-stream concentration distribution, and a power law upstream tail with a slope of -2.2. The BTC exhibits power law tailing with a slope of -2.9. The tail of the spatial distribution is steeper than temporal distributions because the mass retained upstream of the main tracer peak reenters the stream flow at a later time, causing smaller lags (steeper tails) in the BTCs than in the spatial snapshots. Fluctuations become pronounced in the spatial snapshot 4–5 km upstream from the peak and in the BTC tail after 5×10^4 s, because only small amount of tracer mass remains in the sediment bed and returns to the water column at late times. For visual appearance, these are often smoothed using an adaptive kernel technique [*Pedretti and Fernàndez-Garcia*, 2013], but we choose not to do so here.

Velocity and mixing both decrease strongly with depth in the sediments, causing tracer mass in the shallow subsurface to be rapidly exchanged with the water column, while tracer mass in the deeper subsurface is retained for much longer periods of time. Long-term retention of tracer at depth can be clearly seen in the 2-D simulations (Figure 2, top). Note that tracer concentrations are very similar in the water column and shallow subsurface, indicating rapid mixing across the SWI, while tracer mass is predominantly retained in the sediments at a depth of 0.15–0.25 m. Thus, the shallow subsurface, to a depth of $\sim$0.15 m, behaves as if it is well mixed with the overlying flow, while the deeper hyporheic region, below $\sim$0.15 m, is poorly mixed and behaves as a region of long-term storage. The 2-D surface-subsurface continuum results make it clear that the tailing behavior is controlled specifically by the covariance of pore water velocity and vertical mixing.

The location of hyporheic retention is controlled by both the velocity and mixing distributions (equations (5)–(7)), as the appearance of tracer in the subsurface requires delivery of mass from the water column (i.e., hyporheic exchange), while long-term retention occurs only in regions of very slow pore water transport. Tracer propagates rapidly through the interfacial region and is then retained specifically at the location where pore water velocity and mixing decay in the subsurface, at a depth of 0.15–0.25 m. These results indicate that enhanced transport in the shallow subsurface produces rapid flushing of pore water to a depth of $\sim$0.15 m, despite the fact that longitudinal velocity and vertical mixing both decrease over three orders of magnitude in this region. Therefore, the key mixing interface where tracer mass is retained does not occur exactly at the SWI, and instead appears at a depth of $\sim$0.15 m.

To quantify the effects of the velocity and mixing distributions on tracer transport, we calculated velocity autocorrelations [*Box et al*., 2015] of tracer mass at different vertical positions in the surface-subsurface continuum (Figure 3). Autocorrelations were obtained directly from the particle-tracking model results by calculating correlations in the velocity of individual tracer mass elements over a wide range of time lags. Tracer velocities are highly correlated (autocorrelation close to 1) for short time lags because tracer elements remain near their starting position and thus have similar velocities. As time lag increases, there is increasing chance for tracer to move farther from the starting position and thus sample a wider range of downstream velocities. Ultimately, tracer elements reach a decorrelation threshold (autocorrelation close to 0) corresponding to full sampling of the velocity distribution, indicating complete mixing between the surface and subsurface domains. In order to compare the decorrelation time scales for mass elements starting at different vertical positions (y), we define a decorrelation threshold of 0.0527 based on normal time series assumptions [*Box et al*., 2015]. Tracer mass near the SWI experiences higher velocity and mixing than tracer mass deeper in the hyporheic zone, and therefore exhibits shorter decorrelation time scales. The structure of the velocity and mixing profiles (equations (5)–(7)) caused a sharp increase in decorrelation time scale at depths between 0.15 and 0.25 m (Figure 3b), exactly corresponding to the region of long-term solute retention in the subsurface (Figure 2). These findings clarify that rapid mixing in the near-surface hyporheic region causes exchanged mass to be remixed into the water column and propagate downstream at time

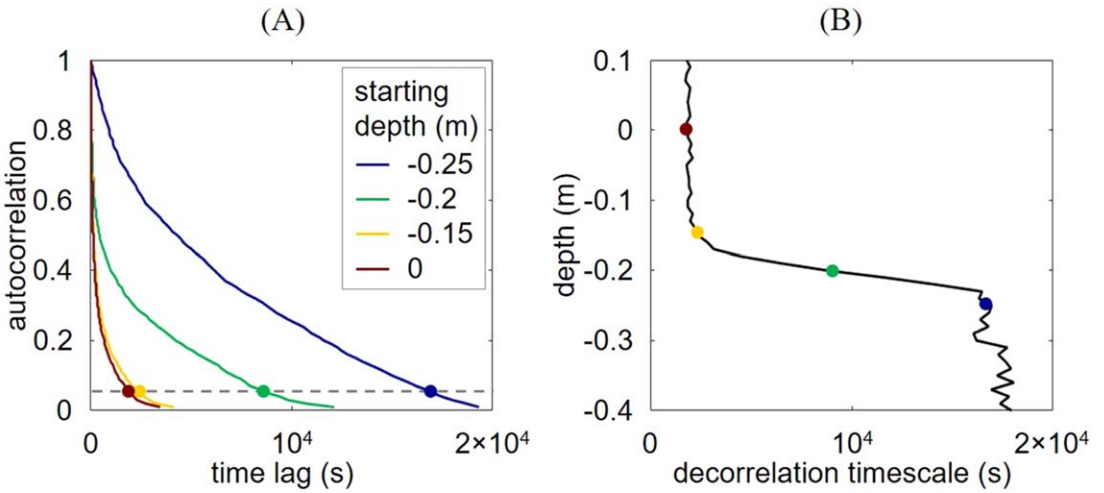

Figure 3. (a) Autocorrelation of tracer mass velocity as a function of the time lag as tracer mass moves downstream. Tracer velocity becomes decorrelated after autocorrelation falls below the decorrelation threshold indicated by the dashed line. (b) Decorrelation time scale as a function of starting position of the tracer mass. Covariation in velocity and mixing causes the velocity decorrelation time scale to increase greatly with depth. Exchanged tracer that propagates to the deeper hyporheic zone is therefore trapped in low-velocity regions for long periods of time.

scales similar to the mean stream flow. However, tracer that penetrates deeper into the sediments is subject to increasingly slow velocities and mixing rates, and hence increasingly long travel times.

3.2. Reactive Tracer Dynamics

Reactive transport in the coupled surface-subsurface domain with uniform, layered, and exponential hyporheic denitrification rate profiles is shown in Figure 4 and supporting information Movies S2–S4. The resulting BTCs and associated whole-stream removal rates, calculated by fitting each BTC with an equivalent uniform hyporheic denitrification profile, are also compared in Figure 5. For the case of uniform hyporheic denitrification (Figure 4a and supporting information Movie S2), nitrate delivered from the stream has the same probability of removal at all depths in the subsurface. Therefore, nitrate removal is controlled only by the rate of delivery from the stream, residence time in the subsurface, and the denitrification rate constant [*Briggs et al*., 2014; *Aubeneau et al*., 2015a]. Subsurface denitrification removes nitrate from the hyporheic zone, and therefore strongly attenuates the mass retained in the subsurface behind the in-stream tracer peak. This removal is reflected in the attenuation of the tail in the 1-D spatial snapshot. Accordingly, less nitrate is exchanged back to the water column, leading to weak tempering of the BTC tail, i.e., a transition from the heavy-tailed power law hyporheic residence time to an exponential decay at the characteristic time scale of the first-order denitrification process [*Meerschaert et al*., 2008; *Aubeneau et al*., 2015a] (Figure 5).

With layered denitrification (Figure 4b and supporting information Movie S3), exchanged nitrate is metabolized at a higher rate in the bioactive layer immediately below the SWI, to a depth of 0.2 m. Rapid flushing of this bioactive region supplies substantial nitrate from the water column, leading to much more rapid removal than the uniform denitrification case. Nitrate that initially propagates through the bioactive layer and is retained deeper in the subsurface must also return through the bioactive interface before being exchanged back to the water column, leading to a second opportunity for hyporheic denitrification. This effectively removes all of the retained mass, which can be seen in the strong tempering of the late-time BTC. Overall, the bioactive layer greatly increases effective reach-average denitrification relative to the uniform case, as shown in Figure 5. This indicates that assumption of a single, homogeneous reach-average uptake rate will yield uncertainty in estimation of hyporheic denitrification rates from analysis of in-stream BTCs.

The exponential denitrification rate profile (Figure 4c and supporting information Movie S4) has a very high denitrification rate just at the SWI and decreases rapidly with depth. The results are therefore similar to the bioactive layer case but show even more extensive removal in the shallow subsurface owing to the faster denitrification rate at the interface. Rapid flushing of the uppermost part of the hyporheic zone therefore yields very fast removal of exchanged reactive tracer. Essentially all of the exchanged mass is removed in the shallow subsurface (depth < 0.1 m), leading to extremely little long-term retention. Within the

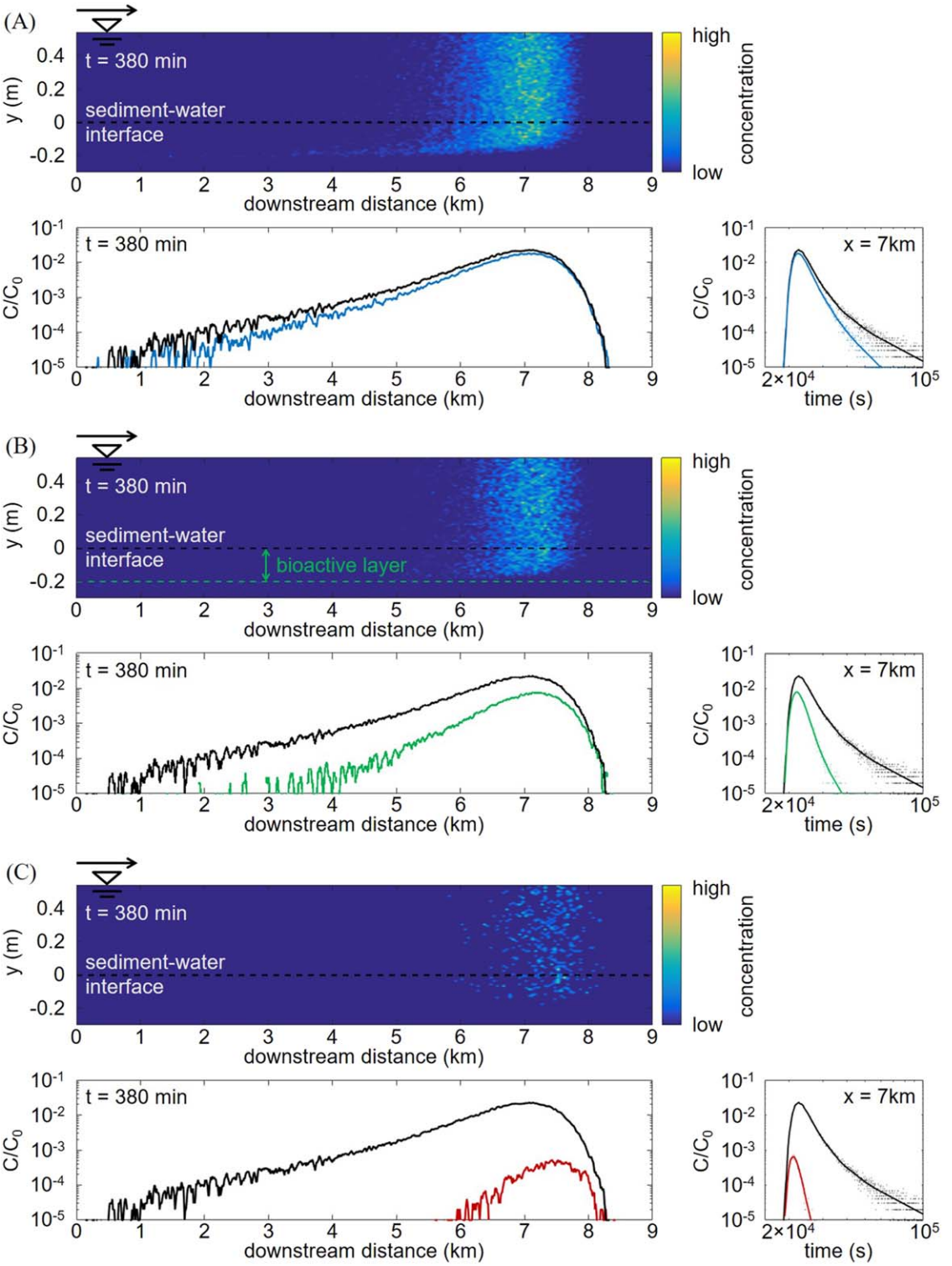

Figure 4. Concentration snapshots and breakthrough curves of reactive tracer under (a) uniform, (b) layered, and (c) exponential hyporheic denitrification profiles. For each case, the top figure shows a heat map of tracer concentration across the entire 2-D domain 380 min after pulse injection into the water column, the bottom left figure shows the corresponding spatial snapshot of in-stream concentration, and the bottom right figure shows in-stream breakthrough curves 7 km downstream of the injection location. Reactive tracer concentrations are shown in blue for the uniform case, green for the layered case, and red for the exponential case. The conservative curves are shown in black for comparison.

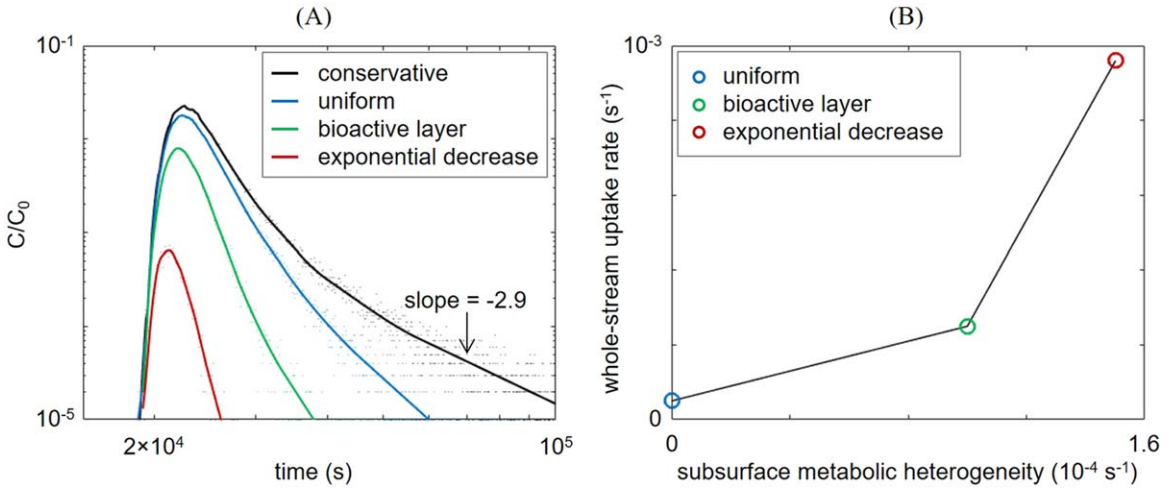

Figure 5. (a) Breakthrough curves of conservative and reactive solutes 7 km downstream of the injection point, and associated whole-stream average denitrification rate constants. The conservative breakthrough curve has a late-time tail with power law slope of −2.9, indicating a wide range of hyporheic storage time scales. Hyporheic denitrification attenuates both the peaks and the tails of breakthrough curves. Increasing denitrification rates in the well-flushed region near the sediment-water interface lead to greater overall attenuation of the breakthrough curve—corresponding to greater reach-scale uptake—and greater tempering of the breakthrough curve tails. (b) Whole-stream uptake rate increases with subsurface denitrification heterogeneity, which is quantified here as the standard deviation of the subsurface denitrification rate profile.

hyporheic zone, exchanged tracer can be found only in the near-surface region that is well mixed with the stream (Figure 2c, top), reflecting short-term persistence of recently exchanged tracer mass, i.e., tracer that has just been delivered from the stream and has not yet had time to be metabolized. Correspondingly, both the 1-D spatial snapshots and BTCs show extremely strong tempering, as mass that would have occurred in the tails has been nearly completely metabolized.

Overall, whole-stream uptake increased substantially where heterogeneity in denitrification resulted in higher rates closer to the SWI. Here, subsurface denitrification heterogeneity was quantified as the standard deviation of the denitrification profile in the subsurface (Figure 6). The whole-stream uptake rate is highest for the exponential hyporheic denitrification profile (9.6×10^{-4} s^{-1}), which has the greatest spatial variability, medium for the layered profile (2.5×10^{-4} s^{-1}), and lowest for the uniform profile (5.0×10^{-5} s^{-1}, just 5% of the exponential case). These results, in concert with the spatial and temporal concentration distributions (Figure 4), indicate that rapid flushing of highly bioactive regions near the SWI is the dominant mechanism of reach-scale uptake. However, this effect is not normally considered in analysis of in-stream tracer injection data. To evaluate the uncertainty associated with ignoring hyporheic heterogeneity, we fit the BTC for each case with an equivalent uniform denitrification profile. This approach assumes that hyporheic denitrification is spatially invariant, which is effectively the same as the assumption of homogeneous hyporheic reaction used in the TSM and nutrient spiraling models. Assuming that hyporheic denitrification is spatially invariant causes the whole-stream uptake rate to be underestimated by a factor of 5.0 when the actual profile is layered, and a factor of 19.2 when the profile is exponential. Conversely, when interpreting in-stream BTCs, assuming that hyporheic denitrification is homogeneous will overestimate the depth-averaged hyporheic denitrification rate by a factor of 5.0 for the layered profile, and a factor of 19.2 for the exponential profile.

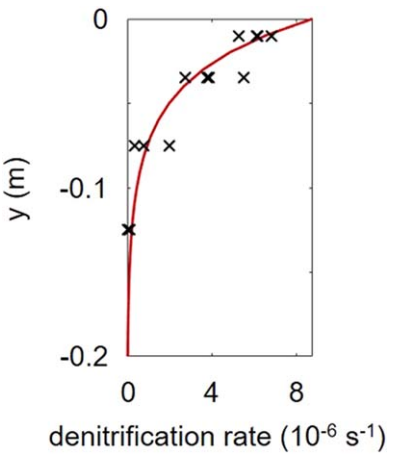

Figure 6. Vertical profile of in situ hyporheic denitrification rate constants in Little Rabbit Creek. Black crosses represent first-order rates converted directly from observed values [*Inwood*, 2004; *Inwood et al*., 2007]. Red line is an exponential fit of the denitrification rate constants.

3.3. Field Application: Nitrogen Dynamics in a Headwater Stream

To demonstrate the influence of subsurface denitrification heterogeneity on whole-stream nitrogen dynamics, we used the model presented above to simulate denitrification in Little

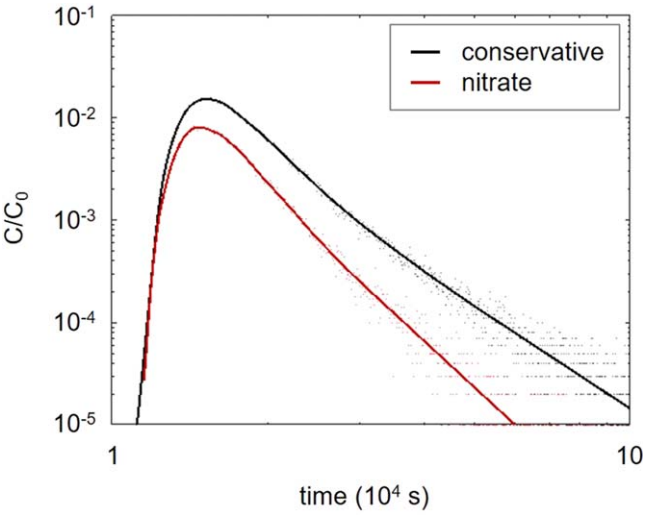

Figure 7. Simulated breakthrough curve of nitrate relative to conservative transport in Little Rabbit Creek at $x = 1$ km. Simulations are based on contemporaneously measured stream flow and carbon-amended hyporheic denitrification (supporting information Table S2 and Figure 6). The overall reach-scale nitrate removal is 48.8%, and the equivalent whole-stream uptake rate of nitrate is 1×10^{-4} s^{-1}. Nitrate is strongly attenuated as a result of effective reach-scale denitrification caused by rapid flushing of the highly bioactive near-surface hyporheic region.

Rabbit Creek, an agricultural headwater stream in the Kalamazoo River Basin (Michigan, USA) [*Inwood et al.*, 2007]. This stream was selected for analysis because it is one of the very few where subsurface patterns in denitrification have been directly measured. Stream morphology and flow parameters are summarized in supporting information Table S2. The streambed is sand with a median grain diameter $D_{50} = 1$ mm [*Arango et al.*, 2007]. We calculated the free surface slope $S = 0.01\%$ from the National Hydrography Dataset [*U.S. Geological Survey*, 2016] and site digital elevation model [*U.S. Geological Survey*, 2013] using ArcGIS 10.3 (ESRI, Redlands, California, USA). Stream flow conditions were measured in October 2002, yielding a mean stream velocity $<u_x> = 0.097$ m/s, river depth $H = 0.088$ m, and river width $W = 2.3$ m [*Inwood*, 2004]. The fact that the river width is much greater than the depth ($W/D = 26$) satisfies the assumptions of our 2-D modeling framework. In absence of direct observations, we used representative values of the slip velocity $U_s = 0.02$ m/s and velocity decay constant $M = 100$ m^{-1} based on values reported for surface-subsurface flow coupling in sand streambeds [*Fries*, 2007; *Higashino et al.*, 2009]. We interpolated vertical dispersion to a depth of 0.05 m below the SWI to capture the effect of near bed turbulence on 50 grain diameters of enhanced exchange in sand beds [*Higashino et al.*, 2009; *Chandler et al.*, 2016]. The mean in-stream velocity estimated using equation (4) was higher than that measured in field, so we calibrated the empirical characteristic length (y_0) in equation (4) to be 1.3×10^{-3} m in order to best match site conditions.

The hyporheic denitrification rate profile was also measured in October 2002 and showed an exponential decrease with depth (Figure 6) [*Inwood*, 2004; *Inwood et al.*, 2007]. We converted the primary denitrification measurements to first-order rate constants, as described in supporting information Text S1. Denitrification rates in Little Rabbit Creek were highly limited by organic carbon in 2002 [*Inwood*, 2004; *Inwood et al.*, 2007] and much lower than hyporheic denitrification rates reported in the literature for other small agricultural streams [*Böhlke et al.*, 2009; *Harvey et al.*, 2013]. We therefore simulated nitrate dynamics with both the observed in situ denitrification rates and carbon-amended denitrification rates, which were experimentally observed to be 25× greater than in situ streambed rates [*Inwood*, 2004; *Inwood et al.*, 2007].

We simulated downstream transport of both nitrate and a conservative solute to demonstrate the effects of the measured patterns in subsurface denitrification on reach-scale nitrate removal. Because hyporheic denitrification in Little Rabbit Creek was highly limited by carbon availability, the nitrate BTC based on in situ denitrification rates shows little attenuation relative to conservative transport even at a downstream distance of 10 km (supporting information Figure S1). These results indicate that hyporheic denitrification has little impact on reach-scale nitrate removal in Little Rabbit Creek under the conditions observed in 2002. This finding is consistent with reach-scale observations from other similar agricultural headwater streams in the Kalamazoo River Basin [*Arango et al.*, 2008]. However, our model simulations predict that carbon amendment will greatly increase reach-scale nitrate removal (Figure 7). Based on the observed increase in hyporheic denitrification following carbon amendment, our model simulations predict 48.8% removal of nitrate in a 1 km reach. For this case, fast denitrification in the top few cm of the streambed rapidly depletes nitrate from exchanged water and eliminates return of nitrate from slow hyporheic transport paths (supporting information Figure S2).

We compared reach-scale effective rate constants for nitrogen uptake both with the observed exponential hyporheic denitrification profile and with an assumption of uniform hyporheic denitrification. The reach-

scale rate for the uniform case was calculated as the depth-averaged hyporheic denitrification rate of the exponential profile. The reach-scale rate for the exponential case was estimated as the uniform hyporheic denitrification rate constant that best fits the observed nitrate BTC. We repeated this analysis for both the observed in situ denitrification rates and the carbon-amended denitrification rates. The effective first-order rate constant for reach-scale nitrate removal is 4×10^{-6} s^{-1} with the measured in situ denitrification rate profile and 1×10^{-4} s^{-1} with the carbon-amended rate profile, but just 6×10^{-7} and 1.7×10^{-5} s^{-1}, respectively, with the assumption of uniform hyporheic denitrification. Directly upscaling local in situ denitrification rates to the reach scale with the assumption of uniform hyporheic denitrification would thus underpredict whole-stream nitrate uptake rates in Little Rabbit Creek by a factor of 6.8. Conversely, incorrectly assuming uniform hyporheic denitrification in the analysis of in-stream BTCs would overestimate the actual depth-averaged hyporheic denitrification rate by a factor of 6.8. The difference between effective reach-scale and in situ rate constants results from the inability of reach-averaged uniform assumptions to adequately distinguish the effects of spatially distributed transport and biogeochemical processes in the hyporheic zone.

4. Discussion

The particle-tracking model presented here combines physically derived probabilistic descriptions of water flow with probabilistic description of hyporheic denitrification. This model formulation is intrinsically mass-conserving, computationally efficient, and does not suffer from the numerical oscillation and dispersion limitations of Eulerian transport models [*Kitanidis*, 1994; *Salamon et al*., 2006; *Robinson et al*., 2010]. Here we used a minimal description of a river that captures basic surface-subsurface coupling: steady and uniform flow, fully developed turbulent flow, smooth flow and mixing distributions over the stream-subsurface continuum, and first-order hyporheic denitrification. Under these basic conditions, the model can be used in real systems to relate local velocity, mixing, and denitrification to reach-scale dynamics. Pore water velocity and mixing decrease with depth in the hyporheic zone. This covariation in velocity and mixing causes the time scale for velocity decorrelation to increase greatly with depth, causing exchanged tracer that propagates to the deeper hyporheic zone to be trapped in low-velocity regions for long periods of time. This type of velocity correlation is a general mechanism of anomalous transport and has been particularly recognized in studies of heterogeneous porous media [*Dentz and Bolster*, 2010; *Datta et al*., 2013; *de Anna et al*., 2013; *Bolster et al*., 2014; *Sund et al*., 2015]. Prior studies of hyporheic exchange have also found that decreasing pore water velocity with depth leads to long hyporheic residence times [*Elliott and Brooks*, 1997b, 1997a; *Cardenas and Jiang*, 2010; *Boano et al*., 2014]. However, prior studies have not considered the general implications of correlated motions across the river-hyporheic continuum. Here we found that strong correlations between hyporheic velocity and mixing cause travel time to increase greatly with depth in the hyporheic zone, even for shallow hyporheic exchange induced by enhanced turbulent transport over depths of just 10–50 sediment grain diameters.

Compared with reach-scale tracer experiments, the simulations presented here not only provide full BTCs including information on the wide range of storage time scales that affect tailing but also provide spatial snapshots that are generally not observable in the field. The stream and shallow subsurface characterized by fast velocity and rapid mixing consistently yield fast downstream transport, and tracer transport through these regions dominates the BTC peak and early-time tailing behavior. Deeper within the hyporheic zone, pore water velocity and mixing decrease by orders of magnitude relative to interfacial conditions, giving rise to long-term retention that controls late-time tailing in tracer BTCs. Long-term tracer retention and the corresponding extended tailing in reach-scale BTCs result from the combination of slow hyporheic velocities and strong velocity autocorrelations caused by slow hyporheic mixing rates. While these results were obtained here for the most basic stream-subsurface flow conditions (logarithmic free-stream velocity profile decaying exponentially to a constant Darcy underflow velocity), the results are generalizable as the correlation mechanism is fully general [*Dentz and Bolster*, 2010; *Le Borgne et al*., 2011; *de Anna et al*., 2013; *Bolster et al*., 2014; *Kang et al*., 2015], river water-column velocities are always much higher than pore water velocities, and hyporheic velocities and mixing rates generally decrease with depth [*Bear*, 1972; *Elliott and Brooks*, 1997b; *Cardenas and Wilson*, 2007; *Worman et al*., 2007; *Cardenas et al*., 2008; *Logan*, 2012; *Cranswick et al*., 2014]. Power law tailing in river BTCs has commonly been attributed to multiscale hyporheic flow patterns and geomorphic complexity [*Cardenas*, 2007; *Gooseff et al*., 2007; *Worman et al*., 2007; *Patil et al*., 2013;

Aubeneau et al., 2015b; *Pryshlak et al*., 2015]. Prior studies have also suggested that shallow hyporheic exchange leads to exponential tailing in in-stream BTCs, while deeper hyporheic exchange leads to power law tailing [*Haggerty et al*., 2002; *Drummond et al*., 2012; *Stonedahl et al*., 2012; *Aubeneau et al*., 2015a]. Here we showed that covariation between velocity and mixing produces broad travel time distributions and late-time power law tailing in in-stream tracer BTCs, even in the absence of geomorphic complexity.

Many ecologically important constituents, especially nitrate and phosphate, are enriched in rivers due to a combination of agricultural, industrial, and municipal discharge [*Turner et al*., 2003; *Allan*, 2004; *Schlesinger et al*., 2006; *Conley et al*., 2009; *Schoumans et al*., 2014; *Withers et al*., 2014]. Unlike phenomenological models that lump physical, chemical, and biological processes into reach-scale calibration parameters, the process-based model presented here explicitly represents vertical patterns in velocity, mixing, and denitrification, and therefore can be used to discriminate the effects of covariations in flow and denitrification on reach-scale nitrogen dynamics. Covariation between patterns of hyporheic flow and denitrification causes exchanged mass with the fastest downstream velocity to be subject to the highest transformation rates, which reduces both the peak and early-time tail in downstream BTCs of injected nitrate. Conversely, late-time tailing in BTCs reflects tracer mass that propagates through the bioactive interface, is retained for a significant amount of time in the deeper sediment, and returns through the bioactive interface to the water column. Because the time scales of hyporheic exchange are very broad, the bioactive interface effectively metabolizes retained mass at all time scales. Further, rapid flushing of the near-surface region relative to the deeper hyporheic zone causes the bioactive interface to have a disproportionally large effect on in-stream nutrient concentrations. This is true for all cases where the transformation rate near the SWI is much greater than at depth (e.g., for both the exponential and bioactive layer cases considered here). Vertical variability in the denitrification rate, with the greatest rate near the rapidly flushing SWI, causes stronger tempering of in-stream BTC and higher reach-scale nitrogen removal. The set of simulations illustrate the general importance of vertical patterns of velocity, mixing, and denitrification on reach-scale nitrogen removal. Our findings are therefore expected to be general for sand and gravel bed rivers and not dependent on the specific values used as simulation conditions.

It should be noted that transformation rates do not always decrease monotonically with depth in the sediments. Denitrification, in particular, is inhibited by the presence of oxygen [*Smith and Tiedje*, 1979; *Kemp and Dodds*, 2002]. Hyporheic exchange of oxygen can yield a shallow oxic layer where nitrification dominates, and an underlying suboxic or anoxic layer where denitrification occurs [*Nielsen et al*., 1990; *Rysgaard et al*., 1998; *Zarnetske et al*., 2011b; *Marzadri et al*., 2012]. The thickness of the oxic sediment layer in aquatic systems ranges from millimeters to centimeters and can even extend to tens of meters along lateral hyporheic flow paths [*Nielsen et al*., 1990; *Seitzinger et al*., 2006; *Clilverd et al*., 2008; *Zarnetske et al*., 2011a]. Nonetheless, available data suggest that the highest rates of denitrification in river sediments generally occur very near the SWI [*Garcia-Ruiz et al*., 1998a; *Inwood et al*., 2007; *Harvey et al*., 2013]. This is likely due to formation of anoxic microsites in benthic biofilms and sediments owing to slow delivery of oxygen from the water column relative to in situ rates of aerobic metabolism [*Vervier et al*., 1992; *Pretty et al*., 2006]. The approach presented here can also be directly applied to solutes other than nitrate, but it is important to recognize that other constituents may exhibit different patterns of hyporheic biogeochemical transformation [*Jones and Mulholland*, 1999; *Boano et al*., 2014; *Battin et al*., 2016]. Thus, while the overall approach presented here is generally valid for coupled stream-hyporheic biogeochemistry, the exact patterns of transformation of stream-derived solutes have to be evaluated for each constituent of interest. Covariation between solute transport and microbial metabolism is generally expected to influence biogeochemical transformation rates in rivers because a number of generally important constituents, such as oxygen and other electron acceptors, are delivered from the water column and play a critical role in structuring the hyporheic environment [*Battin et al*., 2016].

Upscaling of spatially distributed hyporheic processes to reach-scale dynamics has been limited by scarcity of field data on spatial patterns of hyporheic flow and microbially mediated transformations [*Stonedahl et al*., 2010; *Harvey et al*., 2013; *Boano et al*., 2014; *Cardenas*, 2015]. Commonly used models for estimating reach-scale nutrient dynamics, particularly the TSM and Spiraling models, estimate whole-stream uptake rates by fitting in-stream BTCs using reach-average uptake rates that are spatially invariant within reaches [*Boano et al*., 2014]. Hydrological, geomorphological, and ecological controls on reach-scale nutrient processing have most commonly been explored by attempting to correlate whole-stream uptake rates with

individual stream properties such as hyporheic exchange rate, in-stream nutrient concentration, organic matter concentration, and bed sediment size [*Mulholland et al*., 1985; *Hoellein et al*., 2007; *Gibson et al*., 2015; *Rodriguez-Cardona et al*., 2016]. This approach has proven to be very limited: while empirical correlations have captured the effects of major differences in river trophic state and channel morphology, consistent correlations between biogeochemical and hydrological parameters have generally not been found [*Hall et al*., 2002; *Ensign and Doyle*, 2005; *Lautz and Siegel*, 2007; *Boano et al*., 2014]. Recently, *Gomez-Velez et al*. [2015] upscaled denitrification throughout the Mississippi River network by using independent statistical distributions of physically driven flow characteristics and spatially uniform denitrification parameters. At a more local scale, *Trauth et al*. [2014] calculated hyporheic denitrification rates within a 10 m reach using a 3-D computational fluid dynamics model with highly detailed flow structure but uniform denitrification parameters. All of these studies assumed that flow and biogeochemical parameters are independent, and hence involve considerable uncertainty when upscaling reach-scale dynamics [*Boano et al*., 2014]. The results presented here suggest that both correlation-based and physics-based approaches that do not explicitly consider covariations between hydrological and biogeochemical process rates will be unable to adequately relate reach-scale dynamics to spatially distributed processes in the hyporheic zone. In particular, assuming that hyporheic biogeochemical process rates are independent of hyporheic flow patterns will underestimate whole-stream transformation rates for cases where there is high microbial activity just at or below the SWI, in the region where hyporheic exchange is enhanced by turbulent pore water transport.

We used Little Rabbit Creek, an agricultural headwater stream, as an example since this is one of the few locations where spatial patterns in hyporheic denitrification have been directly measured in situ [*Garcia-Ruiz et al*., 1998a; *Inwood et al*., 2007; *Harvey et al*., 2013]. In this stream, the hyporheic denitrification rate decreases exponentially with depth. Our simulations showed that linearly upscaling in situ transformation rates while assuming hyporheic denitrification to be spatially invariant underestimates whole-stream rates by factor of 7. Because conventional reach-scale models are unable to adequately relate reach-scale dynamics to spatially distributed processes in the hyporheic zone, a similar degree of mismatch is expected for all streams and rivers with a well-flushed, highly bioactive layer at the SWI, and more generally in cases where microbially mediated transformation is greatest near the streambed surface and decreases substantially with depth.

Beyond the fundamental profiles of velocity, mixing, and denitrification across the SWI considered here, rivers also exhibit multiscale complexity in patterns of hyporheic flow, microbial communities, and biogeochemical conditions [*Cardenas*, 2008; *Buffington and Tonina*, 2009; *Stonedahl et al*., 2010; *Boano et al*., 2014; *Harvey and Gooseff*, 2015; *Battin et al*., 2016; *Caruso et al*., 2016]. Hyporheic exchange can be driven by a number of factors, including bed forms, logs, aquatic vegetation, and spatial and temporal changes in river channel geometry [*Thibodeaux and Boyle*, 1987; *Nepf*, 2004; *Sawyer et al*., 2011; *Boano et al*., 2014]. Groundwater upwelling reduces hyporheic exchange and shrinks the bioactive layer where denitrification occurs, whereas downwelling extends the hyporheic zone and the region of denitrification [*Storey et al*., 2004; *Fox et al*., 2014; *Trauth et al*., 2014; *Fox et al*., 2016]. Nonetheless, covariation between hyporheic flow and denitrification is still generally found in upwelling and downwelling reaches [*Lansdown et al*., 2014; *Trauth et al*., 2014; *Lansdown et al*., 2015] and is generally expected in sand and gravel bed rivers. Therefore, spatial covariation of the type shown here is generally expected to be important in sand and gravel bed rivers, except for the extreme cases where hyporheic reaction rates are much faster than even the most shallow benthic/hyporheic residence times, such that all nutrients are completely removed from pore water before being exchanged back to the water column.

The results presented here indicate that small-scale ($<$25 cm) spatial covariation between flow and microbially mediated transformations are important for reach-scale biogeochemistry (100$+$ m). Characterizing these features in streams and rivers will require dedicated field campaigns to collect data that adequately resolve both hyporheic flow and transformation processes, as well as development of upscaled models that explicitly consider coupling between these processes. While data are increasingly available on spatial patterns in the transport of conservative tracers and nutrients (e.g., from coinjection of bromide and ^{15}N-labeled nitrate), datasets that include colocated, contemporaneous measurements of hyporheic flow, nutrient transport, and biogeochemical transformations are generally lacking. To better evaluate controls on hyporheic transformation rates and improve prediction of whole-stream uptake rates, we recommend increased synergy of hydrological, biogeochemical, and microbiological field investigations. In particular,

we recommend detailed observations of spatial patterns of pore water transport, microbial activity, and biogeochemical transformation rates throughout the hyporheic zone, because interactions of these processes directly influence large-scale nutrient dynamics. Improved predictions of reach-scale and network-scale nutrient dynamics will then require integrating surface and subsurface measurements with either spatially explicit models or statistical approaches that adequately capture covariations in the underlying process rates. Because it is not possible to directly integrate either hyporheic flow processes or biogeochemical processes over the relevant range of scales in river systems [*Boano et al*., 2014; *Harvey and Gooseff*, 2015], the most feasible approach will likely be to develop a hybrid model with explicit representation of spatial structure to the maximum computationally feasible scale and statistical closure schemes for sub-grid-scale process coupling. The results presented here show that such a multiscale approach for physical-biogeochemical hyporheic process coupling is needed to properly assess relationships between local and upscaled hyporheic process rates in cases where pore water velocity, mixing, and transformation rates covary.

Acknowledgments
We thank Clay Arango and Sarah Inwood for providing field data on denitrification in Little Rabbit Creek. This work was supported by NSF grants EAR-1215898, EAR-1344280, EAR-1351625, EAR-1417264, and EAR-1446236 and the Department of the Army, U.S. Army Research Office grant W911NF-15-1-0569. The content of the information does not necessarily reflect the position or the policy of the federal government, and no official endorsement should be inferred. This research was supported in part through the computational resources and staff contributions provided for the Quest high performance computing facility at Northwestern University which is jointly supported by the Office of the Provost, the Office for Research, and Northwestern University Information Technology. The data used are listed in the supporting information and references.

References

Allan, J. D. (2004), Landscapes and riverscapes: The influence of land use on stream ecosystems, *Annu. Rev. Ecol. Evol. Syst.*, *35*, 257–284.
Aquino, T., A. Aubeneau, and D. Bolster (2015), Peak and tail scaling of breakthrough curves in hydrologic tracer tests, *Adv. Water Resour.*, *78*, 1–8.
Aquino, T., A. Aubeneau, G. Mcgrath, D. Bolster, and S. Rao (2017), Noise-driven return statistics: Scaling and truncation in stochastic storage processes, *Sci. Rep.*, *7*, 302.
Arango, C., J. Tank, L. Johnson, and S. Hamilton (2008), Assimilatory uptake rather than nitrification and denitrification determines nitrogen removal patterns in streams of varying land use, *Limnol. Oceanogr.*, *53*(6), 2558.
Arango, C. P., J. L. Tank, J. L. Schaller, T. V. Royer, M. J. Bernot, and M. B. David (2007), Benthic organic carbon influences denitrification in streams with high nitrate concentration, *Freshwater Biol.*, *52*(7), 1210–1222, doi:10.1111/j.1365-2427.2007.01758.x.
Argerich, A., E. Marti, F. Sabater, M. Ribot, D. Von Schiller, and J. L. Riera (2008), Combined effects of leaf litter inputs and a flood on nutrient retention in a Mediterranean mountain stream during fall, *Limnol. Oceanogr.*, *53*(2), 631–641, doi:10.4319/lo.2008.53.2.0631.
Arnon, S., C. G. Peterson, K. A. Gray, and A. I. Packman (2007), Influence of flow conditions and system geometry on nitrate use by benthic biofilms: Implications for nutrient mitigation, *Environ. Sci. Technol.*, *41*(23), 8142–8148.
Aubeneau, A., B. Hanrahan, D. Bolster, and J. Tank (2014), Substrate size and heterogeneity control anomalous transport in small streams, *Geophys. Res. Lett.*, *41*, 8335–8341, doi:10.1002/2014GL061838.
Aubeneau, A. F., J. D. Drummond, R. Schumer, D. Bolster, J. L. Tank, and A. I. Packman (2015a), Effects of benthic and hyporheic reactive transport on breakthrough curves, *Freshwater Sci.*, *34*(1), 301–315, doi:10.1086/680037.
Aubeneau, A. F., R. L. Martin, D. Bolster, R. Schumer, D. Jerolmack, and A. Packman (2015b), Fractal patterns in riverbed morphology produce fractal scaling of water storage times, *Geophys. Res. Lett.*, *42*, 5309–5315, doi:10.1002/2015GL064155.
Battin, T. J., L. A. Kaplan, S. Findlay, C. S. Hopkinson, E. Marti, A. I. Packman, J. D. Newbold, and F. Sabater (2008), Biophysical controls on organic carbon fluxes in fluvial networks, *Nat. Geosci.*, *1*(2), 95–100, doi:10.1038/ngeo101.
Battin, T. J., K. Besemer, M. M. Bengtsson, A. M. Romani, and A. I. Packmann (2016), The ecology and biogeochemistry of stream biofilms, *Nat. Rev. Microbiol.*, *14*(4), 251–263, doi:10.1038/nrmicro.2016.15.
Bear, J. (1972), *Dynamics of Fluids in Porous Media*, vol. xvii, 764 pp., Am. Elsevier Publ. Co., New York.
Beavers, G. S., and D. D. Joseph (1967), Boundary conditions at a naturally permeable wall, *J. Fluid Mech.*, *30*, 197–207, doi:10.1017/S0022112067001375.
Bellin, A., D. Tonina, and A. Marzadri (2015), Breakthrough curve moments scaling in hyporheic exchange, *Water Resour. Res.*, *51*, 1353–1358, doi:10.1002/2014WR016559.
Bencala, K. E., and R. A. Walters (1983), Simulation of solute transport in a mountain pool-and-riffle stream with a kinetic mass transfer model for sorption, *Water Resour. Res.*, *19*(3), 732–738.
Bencala, K. E., M. N. Gooseff, and B. A. Kimball (2011), Rethinking hyporheic flow and transient storage to advance understanding of stream-catchment connections, *Water Resour. Res.*, *47*, W00H03, doi:10.1029/2010WR010066.
Boano, F., J. W. Harvey, A. Marion, A. I. Packman, R. Revelli, L. Ridolfi, and A. Worman (2014), Hyporheic flow and transport processes: Mechanisms, models, and biogeochemical implications, *Rev. Geophys.*, *52*, 603–679, doi:10.1002/2012RG000417.
Böhlke, J. K., R. C. Antweiler, J. W. Harvey, A. E. Laursen, L. K. Smith, R. L. Smith, and M. A. Voytek (2009), Multi-scale measurements and modeling of denitrification in streams with varying flow and nitrate concentration in the upper Mississippi River basin, USA, *Biogeochemistry*, *93*(1–2), 117–141.
Bolster, D., Y. Meheust, T. Le Borgne, J. Bouquain, and P. Davy (2014), Modeling preasymptotic transport in flows with significant inertial and trapping effects—The importance of velocity correlations and a spatial Markov model, *Adv. Water Resour.*, *70*, 89–103, doi:10.1016/j.advwatres.2014.04.014.
Boudreau, B. P. (2000), The mathematics of early diagenesis: From worms to waves, *Rev. Geophys.*, *38*(3), 389–416, doi:10.1029/2000RG000081.
Box, G. E., G. M. Jenkins, G. C. Reinsel, and G. M. Ljung (2015), *Time Series Analysis: Forecasting and Control*, John Wiley, Hoboken, N. J.
Briggs, M. A., L. K. Lautz, and D. K. Hare (2014), Residence time control on hot moments of net nitrate production and uptake in the hyporheic zone, *Hydrol. Processes*, *28*(11), 3741–3751, doi:10.1002/hyp.9921.
Briggs, M. A., F. D. Day-Lewis, J. P. Zarnetske, and J. W. Harvey (2015), A physical explanation for the development of redox microzones in hyporheic flow, *Geophys. Res. Lett.*, *42*, 4402–4410, doi:10.1002/2015GL064200.
Buffington, J. M., and D. Tonina (2009), Hyporheic exchange in mountain rivers II: Effects of channel morphology on mechanics, scales, and rates of exchange, *Geogr. Compass*, *3*(3), 1038–1062.
Camarena, C., D. Otero, and J. H. Ren (2016), Modelling and experimental study of coupled exchange of p,p-DDE and colloids in a flume simulated stream-streambed system, *Hydrol. Processes*, *30*(1), 40–56, doi:10.1002/hyp.10560.

Cardenas, M. B. (2007), Potential contribution of topography-driven regional groundwater flow to fractal stream chemistry: Residence time distribution analysis of Tóth flow, *Geophys. Res. Lett.*, *34*, L05403, doi:10.1029/2006GL029126.
Cardenas, M. B. (2008), Surface water-groundwater interface geomorphology leads to scaling of residence times, *Geophys. Res. Lett.*, *35*, L08402, doi:10.1029/2008GL033753.
Cardenas, M. B. (2015), Hyporheic zone hydrologic science: A historical account of its emergence and a prospectus, *Water Resour. Res.*, *51*, 3601–3616, doi:10.1002/2015WR017028.
Cardenas, M. B., and X. W. Jiang (2010), Groundwater flow, transport, and residence times through topography-driven basins with exponentially decreasing permeability and porosity, *Water Resour. Res.*, *46*, W11538, doi:10.1029/2010WR009370.
Cardenas, M. B., and J. L. Wilson (2007), Hydrodynamics of coupled flow above and below a sediment-water interface with triangular bedforms, *Adv. Water Resour.*, *30*(3), 301–313, doi:10.1016/j.advwatres.2006.06.009.
Cardenas, M. B., J. L. Wilson, and R. Haggerty (2008), Residence time of bedform-driven hyporheic exchange, *Adv. Water Resour.*, *31*(10), 1382–1386, doi:10.1016/j.advwatres.2008.07.006.
Caruso, A., L. Ridolfi, and F. Boano (2016), Impact of watershed topography on hyporheic exchange, *Adv. Water Resour.*, *94*, 400–411.
Chandler, I., I. Guymer, J. M. Pearson, and R. Van Egmond (2016), Vertical variation of mixing within porous sediment beds below turbulent flows, *Water Resour. Res.*, *52*, 3493–3509, doi:10.1002/2015WR018274.
Chislock, M. F., E. Doster, R. A. Zitomer, and A. Wilson (2013), Eutrophication: Causes, consequences, and controls in aquatic ecosystems, *Nat. Educ. Knowledge*, *4*(4), 10.
Christensen, P. B., L. P. Nielsen, J. Sorensen, and N. P. Revsbech (1990), Denitrification in nitrate-rich streams: Diurnal and seasonal variation related to benthic oxygen metabolism, *Limnol. Oceanogr.*, *35*(3), 640–651.
Clilverd, H. M., J. B. Jones, and K. Kielland (2008), Nitrogen retention in the hyporheic zone of a glacial river in interior Alaska, *Biogeochemistry*, *88*(1), 31–46.
Conley, D. J., H. W. Paerl, R. W. Howarth, D. F. Boesch, S. P. Seitzinger, K. E. Havens, C. Lancelot, and G. E. Likens (2009), Controlling eutrophication: Nitrogen and phosphorus, *Science*, *323*(5917), 1014–1015, doi:10.1126/science.1167755.
Conley, D. J., et al. (2011), Hypoxia is increasing in the coastal zone of the Baltic Sea, *Environ. Sci. Technol.*, *45*(16), 6777–6783, doi:10.1021/es201212r.
Costerton, J. W., and H. M. Lappin-Scott (1995), Introduction to microbial biofilms, in *Microb. Biofilms*, pp. 1–11, Cambridge University Press, Cambridge, U. K.
Covino, T. P., B. L. Mcglynn, and R. A. Mcnamara (2010), Tracer Additions for Spiraling Curve Characterization (TASCC): Quantifying stream nutrient uptake kinetics from ambient to saturation, *Limnol. Oceanogr. Methods*, *8*, 484–498, doi:10.4319/lom.2010.8.484.
Craft, J. A., J. A. Stanford, and M. Pusch (2002), Microbial respiration within a floodplain aquifer of a large gravel-bed river, *Freshwater Biol.*, *47*(2), 251–261.
Cranswick, R. H., P. G. Cook, M. Shanafield, and S. Lamontagne (2014), The vertical variability of hyporheic fluxes inferred from riverbed temperature data, *Water Resour. Res.*, *50*, 3994–4010, doi:10.1002/2013WR014410.
Datta, S. S., H. Chiang, T. S. Ramakrishnan, and D. A. Weitz (2013), Spatial fluctuations of fluid velocities in flow through a three-dimensional porous medium, *Phys. Rev. Lett.*, *111*(6), 5, doi:10.1103/PhysRevLett.111.064501.
De Anna, P., T. Le Borgne, M. Dentz, A. M. Tartakovsky, D. Bolster, and P. Davy (2013), Flow intermittency, dispersion, and correlated continuous time random walks in porous media, *Phys. Rev. Lett.*, *110*(18), 5, doi:10.1103/PhysRevLett.110.184502.
Delay, F., P. Ackerer, and C. Danquigny (2005), Simulating solute transport in porous or fractured formations using random walk particle tracking: A review, *Vadose Zone J.*, *4*(2), 360–379, doi:10.2136/vzj2004.0125.
Dentz, M., and D. Bolster (2010), Distribution- versus correlation-induced anomalous transport in quenched random velocity fields, *Phys. Rev. Lett.*, *105*(24), 4, doi:10.1103/PhysRevLett.105.244301.
Diaz, R. J., and R. Rosenberg (2008), Spreading dead zones and consequences for marine ecosystems, *Science*, *321*(5891), 926–929, doi:10.1126/science.1156401.
Drummond, J. D., T. P. Covino, A. F. Aubeneau, D. Leong, S. Patil, R. Schumer, and A. I. Packman (2012), Effects of solute breakthrough curve tail truncation on residence time estimates: A synthesis of solute tracer injection studies, *J. Geophys. Res.*, *117*,*11*, doi:10.1029/2012JG002019.
Elder, J. (1959), The dispersion of marked fluid in turbulent shear flow, *J. Fluid Mech.*, *5*(4), 544–560.
Elliott, A. H., and N. H. Brooks (1997a), Transfer of nonsorbing solutes to a streambed with bed forms: Laboratory experiments, *Water Resour. Res.*, *33*(1), 137–151.
Elliott, A. H., and N. H. Brooks (1997b), Transfer of nonsorbing solutes to a streambed with bed forms: Theory, *Water Resour. Res.*, *33*(1), 123–136, doi:10.1029/96WR02784.
Ensign, S., and M. Doyle (2005), In-channel transient storage and associated nutrient retention: Evidence from experimental manipulations, *Limnol. Oceanogr.*, *50*(6), 1740–1751.
Fabian, M. W., T. A. Endreny, A. Bottacin-Busolin, and L. K. Lautz (2011), Seasonal variation in cascade-driven hyporheic exchange, northern Honduras, *Hydrol. Processes*, *25*(10), 1630–1646, doi:10.1002/hyp.7924.
Fellows, C. S., M. H. Valett, and C. N. Dahm (2001), Wholestream metabolism in two montane streams: Contribution of the hyporheic zone, *Limnol. Oceanogr.*, *46*(3), 523–531.
Fischer, H., F. Kloep, S. Wilzcek, and M. T. Pusch (2005), A river's liver—Microbial processes within the hyporheic zone of a large lowland river, *Biogeochemistry*, *76*(2), 349–371, doi:10.1007/s10533-005-6896-y.
Fischer, H. B. (1979), *Mixing in Inland and Coastal Waters*, vol. xiv, 483 pp., Academic, New York.
Fischer, H. B., J. E. List, C. R. Koh, J. Imberger, and N. H. Brooks (1979), *Mixing in Inland and Coastal Waters*, Academic, San Diego, Calif.
Fox, A., F. Boano, and S. Arnon (2014), Impact of losing and gaining streamflow conditions on hyporheic exchange fluxes induced by dune-shaped bed forms, *Water Resour. Res.*, *50*, 1895–1907, doi:10.1002/2013WR014668.
Fox, A., G. Laube, C. Schmidt, J. Fleckenstein, and S. Arnon (2016), The effect of losing and gaining flow conditions on hyporheic exchange in heterogeneous streambeds, *Water Resour. Res.*, *52*, 7460–7477, doi:10.1002/2016WR018677.
Fries, J. S. (2007), Predicting interfacial diffusion coefficients for fluxes across the sediment-water interface, *J. Hydraul. Eng.*, *133*(3), 267–272.
Garcia-Ruiz, R., S. N. Pattinson, and B. A. Whitton (1998a), Denitrification and nitrous oxide production in sediments of the Wiske, a lowland eutrophic river, *Sci. Total Environ.*, *210*(1–6), 307–320, doi:10.1016/S0048-9697(98)00020-5.
Garcia-Ruiz, R., S. N. Pattinson, and B. A. Whitton (1998b), Denitrification in river sediments: Relationship between process rate and properties of water and sediment, *Freshwater Biol.*, *39*(3), 467–476.
Gibson, C. A., C. M. O'reilly, A. L. Conine, and S. M. Lipshutz (2015), Nutrient uptake dynamics across a gradient of nutrient concentrations and ratios at the landscape scale, *J. Geophys. Res. Biogeosci.*, *120*, 326–340, doi:10.1002/2014JG002747.

Gomez-Velez, J. D., J. Harvey, M. B. Cardenas, and B. Kiel (2015), Denitrification in the Mississippi River network controlled by flow through river bedforms, *Nat. Geosci.*, *8*(12), 941–U975, doi:10.1038/ngeo2567.
González-Pinzón, R., R. Haggerty, and M. Dentz (2013), Scaling and predicting solute transport processes in streams, *Water Resour. Res.*, *49*, 4071–4088, doi:10.1002/wrcr.20280.
Gooseff, M. N., J. K. Anderson, S. M. Wondzell, J. Lanier, and R. Haggerty (2006), A modelling study of hyporheic exchange pattern and the sequence, size, and spacing of stream bedforms in mountain stream networks, Oregon, USA, *Hydrol. Processes*, *20*(11), 2443–2457.
Gooseff, M. N., R. O. Hall, and J. L. Tank (2007), Relating transient storage to channel complexity in streams of varying land use in Jackson Hole, Wyoming, *Water Resour. Res.*, *43*, 10, doi:10.1029/2005WR004626.
Habel, F., C. Mendoza, and A. C. Bagtzoglou (2002), Solute transport in open channel flows and porous streambeds, *Adv. Water Resour.*, *25*(4), 455–469, doi:10.1016/S0309-1708(01)00052-5.
Haggerty, R., S. M. Wondzell, and M. A. Johnson (2002), Power-law residence time distribution in the hyporheic zone of a 2nd-order mountain stream, *Geophys. Res. Lett.*, *29*(13), doi:10.1029/2002GL014743.
Hall, R., E. Bernhardt, and G. Likens (2002), Relating nutrient uptake with transient storage in forested mountain streams, *Limnol. Oceanogr.*, *47*(1), 255–265.
Harman, C., A. Ward, and A. Ball (2016), How does reach-scale stream-hyporheic transport vary with discharge? Insights from rSAS analysis of sequential tracer injections in a headwater mountain stream, *Water Resour. Res.*, *52*, 7130–7150, doi:10.1002/2016WR018832.
Harvey, J., and M. Gooseff (2015), River corridor science: Hydrologic exchange and ecological consequences from bedforms to basins, *Water Resour. Res.*, *51*, 6893–6922, doi:10.1002/2015WR017617.
Harvey, J. W., and B. J. Wagner (2000), *Quantifying Hydrologic Interactions Between Streams and Their Subsurface Hyporheic Zones*, Academic, San Diego, Calif.
Harvey, J. W., J. K. Bohlke, M. A. Voytek, D. Scott, and C. R. Tobias (2013), Hyporheic zone denitrification: Controls on effective reaction depth and contribution to whole-stream mass balance, *Water Resour. Res.*, *49*, 6298–6316, doi:10.1002/wrcr.20492.
Herrman, K. S., V. Bouchard, and R. H. Moore (2008), An assessment of nitrogen removal from headwater streams in an agricultural watershed, northeast Ohio, USA, *Limnol. Oceanogr.*, *53*(6), 2573–2582, doi:10.4319/lo.2008.53.6.2573.
Higashino, M., J. J. Clark, and H. G. Stefan (2009), Pore water flow due to near-bed turbulence and associated solute transfer in a stream or lake sediment bed, *Water Resour. Res.*, *45*, W12414, doi:10.1029/2008WR007374.
Hoellein, T. J., J. L. Tank, E. J. Rosi-Marshall, S. A. Entrekin, and G. A. Lamberti (2007), Controls on spatial and temporal variation of nutrient uptake in three Michigan headwater streams, *Limnol. Oceanogr.*, *52*(5), 1964–1977.
Inwood, S. E. (2004), The influence of land use on denitrification in headwater streams in the Kalamazoo River Watershed, Michigan, MS thesis, Dep. of Biol. Sci., Univ. of Notre Dame, Notre Dame, Indiana.
Inwood, S. E., J. L. Tank, and M. J. Bernot (2007), Factors controlling sediment denitrification in midwestern streams of varying land use, *Microb. Ecol.*, *53*(2), 247–258, doi:10.1007/s00248-006-9104-2.
Jones, J. B., and P. J. Mulholland (1999), *Streams and Ground Waters*, Academic, San Diego, Calif.
Kang, P. K., T. Le Borgne, M. Dentz, O. Bour, and R. Juanes (2015), Impact of velocity correlation and distribution on transport in fractured media: Field evidence and theoretical model, *Water Resour. Res.*, *51*, 940–959, doi:10.1002/2014WR015799.
Kemp, M. J., and W. K. Dodds (2002), The influence of ammonium, nitrate, and dissolved oxygen concentrations on uptake, nitrification, and denitrification rates associated with prairie stream substrata, *Limnol. Oceanogr.*, *47*(5), 1380–1393.
Kinzelbach, W. (1988), The random walk method in pollutant transport simulation, in *Groundwater Flow and Quality Modelling*, pp. 227–245, D. Reidel Publ. Co., Norwell, Mass.
Kitanidis, P. K. (1994), Particle-tracking equations for the solution of the advection-dispersion equation with variable coefficients, *Water Resour. Res.*, *30*(11), 3225–3227, doi:10.1029/94WR01880.
Lansdown, K., M. Trimmer, C. Heppell, F. Sgouridis, S. Ullah, A. Heathwaite, A. Binley, and H. Zhang (2012), Characterization of the key pathways of dissimilatory nitrate reduction and their response to complex organic substrates in hyporheic sediments, *Limnol. Oceanogr.*, *57*(2), 387–400.
Lansdown, K., C. M. Heppell, M. Dossena, S. Ullah, A. L. Heathwaite, A. Binley, H. Zhang, and M. Trimmer (2014), Fine-scale in situ measurement of riverbed nitrate production and consumption in an armored permeable riverbed, *Environ. Sci. Technol.*, *48*(8), 4425–4434.
Lansdown, K., C. Heppell, M. Trimmer, A. Binley, A. Heathwaite, P. Byrne, and H. Zhang (2015), The interplay between transport and reaction rates as controls on nitrate attenuation in permeable, streambed sediments, *J. Geophys. Res. Biogeosci.*, *120*, 1093–1109, doi:10.1002/2014JG002874.
Lautz, L., and D. Siegel (2007), The effect of transient storage on nitrate uptake lengths in streams: An inter-site comparison, *Hydrol. Processes*, *21*(26), 3533–3548, doi:10.1002/hyp.6569.
Le Borgne, T., D. Bolster, M. Dentz, P. De Anna, and A. Tartakovsky (2011), Effective pore-scale dispersion upscaling with a correlated continuous time random walk approach, *Water Resour. Res.*, *47*, W12538, doi:10.1029/2011WR010457.
Lefebvre, S., P. Marmonier, and G. Pinay (2004), Stream regulation and nitrogen dynamics in sediment interstices: Comparison of natural and straightened sectors of a third-order stream, *River Res. Appl.*, *20*(5), 499–512.
Logan, B. E. (2012), *Environmental Transport Processes*, John Wiley, Hoboken, N. J.
Lovley, D. R., and F. H. Chapelle (1995), Deep subsurface microbial processes, *Rev. Geophys.*, *33*(3), 365–381, doi:10.1029/95RG01305.
Manes, C., D. Pokrajac, V. I. Nikora, L. Ridolfi, and D. Poggi (2011), Turbulent friction in flows over permeable walls, *Geophys. Res. Lett.*, *38*, L03402, doi:10.1029/2010GL045695.
Marion, A., and M. Zaramella (2005), A residence time model for stream-subsurface exchange of contaminants, *Acta Geophys. Polonica*, *53*(4), 527.
Marzadri, A., D. Tonina, A. Bellin, G. Vignoli, and M. Tubino (2010), Semianalytical analysis of hyporheic flow induced by alternate bars, *Water Resour. Res.*, *46*, W07531, doi:10.1029/2009WR008285.
Marzadri, A., D. Tonina, and A. Bellin (2012), Morphodynamic controls on redox conditions and on nitrogen dynamics within the hyporheic zone: Application to gravel bed rivers with alternate-bar morphology, *J. Geophys. Res.*, *117*, G00N10, doi:10.1029/2012JG001966.
Marzadri, A., D. Tonina, A. Bellin, and J. Tank (2014), A hydrologic model demonstrates nitrous oxide emissions depend on streambed morphology, *Geophys. Res. Lett.*, *41*, 5484–5491, doi:10.1002/2014GL060732.
McClain, M. E., et al. (2003), Biogeochemical hot spots and hot moments at the interface of terrestrial and aquatic ecosystems, *Ecosystems*, *6*(4), 301–312, doi:10.1007/s10021-003-0161-9.
Meerschaert, M. M., Y. Zhang, and B. Baeumer (2008), Tempered anomalous diffusion in heterogeneous systems, *Geophys. Res. Lett.*, *35*, L17403, doi:10.1029/2008GL034899.

Mendoza, C., and D. H. Zhou (1992), Effects of porous bed on turbulent stream flow above bed, *J. Hydraul. Eng.*, *118*(9), 1222–1240, doi:10.1061/(ASCE)0733-9429(1992)118:9(1222).
Merill, L., and D. J. Tonjes (2014), A review of the hyporheic zone, stream restoration, and means to enhance denitrification, *Crit. Rev. Environ. Sci. Technol.*, *44*(21), 2337–2379.
Mulholland, P. J., J. D. Newbold, J. W. Elwood, L. A. Ferren, and J. R. Webster (1985), Phosphorus spiralling in a woodland stream: Seasonal variations, *Ecology*, *66*(3), 1012–1023, doi:10.2307/1940562.
Mulholland, P. J., et al. (2008), Stream denitrification across biomes and its response to anthropogenic nitrate loading, *Nature*, *452*(7184), 202–246, doi:10.1038/nature06686.
Nagaoka, H., and S. Ohgaki (1990), Mass transfer mechanism in a porous riverbed, *Water Res.*, *24*(4), 417–425, doi:10.1016/0043-1354(90)90223-S.
Nepf, H. (2004), Vegetated flow dynamics, in *The Ecogeomorphology of Tidal Marshes*, pp. 137–163, AGU, Washington, D. C.
Newbold, J., P. Mulholland, J. Elwood, and R. O'neill (1982), Organic carbon spiralling in stream ecosystems, *Oikos*, *38*, 266–272.
Newbold, J. D., J. W. Elwood, R. V. Oneill, and W. Vanwinkle (1981), Measuring nutrient spiralling in streams, *Can. J. Fish. Aquat. Sci.*, *38*(7), 860–863.
Nielsen, L. P., P. B. Christensen, N. P. Revsbech, and J. Sorensen (1990), Denitrification and photosynthesis in stream sediment studied with microsensor and wholecore techniques, *Limnol. Oceanogr.*, *35*(5), 1135–1144.
O'Connor, B. L., and J. W. Harvey (2008), Scaling hyporheic exchange and its influence on biogeochemical reactions in aquatic ecosystems, *Water Resour. Res.*, *44*, W12423, doi:10.1029/2008WR007160.
O'Connor, B. L., and M. Hondzo (2007), Enhancement and inhibition of denitrification by fluid-flow and dissolved oxygen flux to stream sediments, *Environ. Sci. Technol.*, *42*(1), 119–125.
O'Connor, B. L., and M. Hondzo (2008), Dissolved oxygen transfer to sediments by sweep and eject motions in aquatic environments, *Limnol. Oceanogr.*, *53*(2), 566.
O'Connor, B. L., M. Hondzo, and J. W. Harvey (2010), Predictive modeling of transient storage and nutrient uptake: Implications for stream restoration, *J. Hydraul. Eng.*, *136*(12), 1018–1032, doi:10.1061/(ASCE)HY.1943-7900.0000180.
Packman, A., M. Salehin, and M. Zaramella (2004), Hyporheic exchange with gravel beds: Basic hydrodynamic interactions and bedform-induced advective flows, *J. Hydraul. Eng.*, *130*(7), 647–656, doi:10.1061/(ASCE)0733-9429(2004)130:7(647).
Packman, A. I., and J. S. MacKay (2003), Interplay of stream-subsurface exchange, clay particle deposition, and streambed evolution, *Water Resour. Res.*, *39*(4), 1097, doi:10.1029/2002WR001432.
Patil, S., T. P. Covino, A. I. Packman, B. L. Mcglynn, J. D. Drummond, R. A. Payn, and R. Schumer (2013), Intrastream variability in solute transport: Hydrologic and geomorphic controls on solute retention, *J. Geophys. Res. Earth Surf.*, *118*, 413–422, doi:10.1029/2012JF002455.
Pedretti, D., and D. Fernàndez-Garcia (2013), An automatic locally-adaptive method to estimate heavily-tailed breakthrough curves from particle distributions, *Adv. Water Resour.*, *59*, 52–65.
Peterson, B. J., W. M. Wollheim, P. J. Mulholland, J. R. Webster, J. L. Meyer, J. L. Tank, E. Martí, W. B. Bowden, H. M. Valett, and A. E. Hershey (2001), Control of nitrogen export from watersheds by headwater streams, *Science*, *292*(5514), 86–90.
Pretty, J. L., A. G. Hildrew, and M. Trimmer (2006), Nutrient dynamics in relation to surface-subsurface hydrological exchange in a groundwater fed chalk stream, *J. Hydrol.*, *330*(1–2), 84–100, doi:10.1016/j.jhydrol.2006.04.013.
Prickett, T. A., T. G. Naymik, C. G. Lonnquist, and I. S. W. Survey (1981), *A "random-Walk" Solute Transport Model for Selected Groundwater Quality Evaluations*, Ill. State Water Surv., Champaign, Ill.
Pryshlak, T. T., A. H. Sawyer, S. H. Stonedahl, and M. R. Soltanian (2015), Multiscale hyporheic exchange through strongly heterogeneous sediments, *Water Resour. Res.*, *51*, 9127–9140, doi:10.1002/2015WR017293.
Rabalais, N., R. Díaz, L. Levin, R. Turner, D. Gilbert, and J. Zhang (2009), Dynamics and distribution of natural and human-caused coastal hypoxia, *Biogeosci. Discuss.*, *6*(5), 9359.
Rehg, K. J., A. I. Packman, and J. H. Ren (2005), Effects of suspended sediment characteristics and bed sediment transport on streambed clogging, *Hydrol. Processes*, *19*(2), 413–427, doi:10.1002/hyp.5540.
Ren, J. H., and A. I. Packman (2002), Effects of background water composition on stream-subsurface exchange of submicron colloids, *J. Environ. Eng.*, *128*(7), 624–634, doi:10.1061/(ASCE)0733-9372(2002)128:7(624).
Robinson, B. A., Z. V. Dash, and G. Srinivasan (2010), A particle tracking transport method for the simulation of resident and flux-averaged concentration of solute plumes in groundwater models, *Comput. Geosci.*, *14*(4), 779–792, doi:10.1007/s10596-010-9190-6.
Rodriguez-Cardona, B., A. S. Wymore, and W. H. Mcdowell (2016), DOC:NO_3^- ratios and NO_3^- uptake in forested headwater streams, *J. Geophys. Res. Biogeosci.*, *121*, 205–217, doi:10.1002/2015JG003146.
Roley, S. S., J. L. Tank, and M. A. Williams (2012), Hydrologic connectivity increases denitrification in the hyporheic zone and restored floodplains of an agricultural stream, *J. Geophys. Res.*, *117*, G00N04, doi:10.1029/2012JG001950.
Runkel, R. L. (1998), *One-Dimensional Transport With Inflow and Storage (OTIS): A Solute Transport Model for Streams and Rivers*, U.S. Dep. of the Inter., U.S. Geol. Surv., Denver, Colo.
Rysgaard, S., B. Thamdrup, N. Risgaard-Petersen, H. Fossing, P. Berg, P. B. Christensen, and T. Dalsgaard (1998), Seasonal carbon and nutrient mineralization in a high-Arctic coastal marine sediment, Young Sound, Northeast Greenland, *Mar. Ecol. Prog. Ser.*, *175*, 261–276, doi:10.3354/meps175261.
Salamon, P., D. Fernandez-Garcia, and J. J. Gomez-Hernandez (2006), A review and numerical assessment of the random walk particle tracking method, *J. Contam. Hydrol.*, *87*(3–4), 277–305, doi:10.1016/j.jconhyd.2006.05.005.
Savant, S. A., D. D. Reible, and L. J. Thibodeaux (1987), Convective transport within stable river sediments, *Water Resour. Res.*, *23*(9), 1763–1768, doi:10.1029/WR023i009p01763.
Sawyer, A. H. (2015), Enhanced removal of groundwater-borne nitrate in heterogeneous aquatic sediments, *Geophys. Res. Lett.*, *42*, 403–410, doi:10.1002/2014GL062234.
Sawyer, A. H., M. B. Cardenas, and J. Buttles (2011), Hyporheic exchange due to channel-spanning logs, *Water Resour. Res.*, *47*, W08502, doi:10.1029/2011WR010484.
Schlesinger, W. H., K. H. Reckhow, and E. S. Bernhardt (2006), Global change: The nitrogen cycle and rivers, *Water Resour. Res.*, *42*, W03S06, doi:10.1029/2005WR004300.
Schmadel, N. M., et al. (2016), Stream solute tracer timescales changing with discharge and reach length confound process interpretation, *Water Resour. Res.*, *52*, 3227–3245, doi:10.1002/2015WR018062.
Schoumans, O. F., W. J. Chardon, M. E. Bechmann, C. Gascuel-Odoux, G. Hofman, B. Kronvang, G. H. Rubaek, B. Ulen, and J. M. Dorioz (2014), Mitigation options to reduce phosphorus losses from the agricultural sector and improve surface water quality: A review, *Sci. Total Environ.*, *468*, 1255–1266, doi:10.1016/j.scitotenv.2013.08.061.

Seitzinger, S. (2008), Nitrogen cycle—Out of reach, *Nature*, *452*(7184), 162–163, doi:10.1038/452162a.
Seitzinger, S., J. A. Harrison, J. K. Bohlke, A. F. Bouwman, R. Lowrance, B. Peterson, C. Tobias, and G. Van Drecht (2006), Denitrification across landscapes and waterscapes: A synthesis, *Ecol. Appl.*, *16*(6), 2064–2090, doi:10.1890/1051–0761(2006)016[2064:DALAWA]2.0.CO;2.
Sheibley, R. W., A. P. Jackman, J. H. Duff, and F. J. Triska (2003), Numerical modeling of coupled nitrification–denitrification in sediment perfusion cores from the hyporheic zone of the Shingobee River, MN, *Adv. Water Resour.*, *26*(9), 977–987.
Smith, M. S., and J. M. Tiedje (1979), Phases of denitrification following oxygen depletion in soil, *Soil Biol. Biochem.*, *11*(3), 261–267, doi:10.1016/0038-0717(79)90071-3.
Stelzer, R. S., L. A. Bartsch, W. B. Richardson, and E. A. Strauss (2011), The dark side of the hyporheic zone: Depth profiles of nitrogen and its processing in stream sediments, *Freshwater Biol.*, *56*(10), 2021–2033, doi:10.1111/j.1365-2427.2011.02632.x.
Stonedahl, S. H., J. W. Harvey, A. Worman, M. Salehin, and A. I. Packman (2010), A multiscale model for integrating hyporheic exchange from ripples to meanders, *Water Resour. Res.*, *46*, W12539, doi:10.1029/2009WR008865.
Stonedahl, S. H., J. W. Harvey, J. Detty, A. Aubeneau, and A. I. Packman (2012), Physical controls and predictability of stream hyporheic flow evaluated with a multiscale model, *Water Resour. Res.*, *48*, W10513, doi:10.1029/2011WR011582.
Storey, R. G., D. D. Williams, and R. R. Fulthorpe (2004), Nitrogen processing in the hyporheic zone of a pastoral stream, *Biogeochemistry*, *69*(3), 285–313.
Sund, N. L., D. Bolster, and C. Dawson (2015), Upscaling transport of a reacting solute through a periodically converging-diverging channel at pre-asymptotic times, *J. Contam. Hydrol.*, *182*, 1–15, doi:10.1016/j.jconhyd.2015.08.003.
Taylor, G. (1954), The dispersion of matter in turbulent flow through a pipe, paper presented at the Royal Society of London A: Mathematical, Physical and Engineering Sciences, The R. Soc., London.
Thibodeaux, L. J., and J. D. Boyle (1987), Bedform-generated convective transport in bottom sediment, *Nature*, *325*(6102), 341–343, doi:10.1038/325341a0.
Trauth, N., C. Schmidt, M. Vieweg, U. Maier, and J. H. Fleckenstein (2014), Hyporheic transport and biogeochemical reactions in pool-riffle systems under varying ambient groundwater flow conditions, *J. Geophys. Res. Biogeosci.*, *119*, 910–928, doi:10.1002/2013JG002586.
Triska, F. J., V. C. Kennedy, R. J. Avanzino, G. W. Zellweger, and K. E. Bencala (1989), Retention and transport of nutrients in a third-order stream in Northwestern California: Hyporheic processes, *Ecology*, *70*(6), 1893–1905, doi:10.2307/1938120.
Turner, R. E., N. N. Rabalais, D. Justic, and Q. Dortch (2003), Global patterns of dissolved N, P and Si in large rivers, *Biogeochemistry*, *64*(3), 297–317.
U.S. Geological Survey (2013), *USGS NED n43w086 1 Arc-Second 2013 1 × 1 Degree ArcGrid*, Reston, Va. [Available at https://www.sciencebase.gov/catalog/item/531e42f0e4b0c9f943a0197d.]
U.S. Geological Survey (2016), *USGS National Hydrography Dataset (NHD) Best Resolution for Michigan 20160412 State or Territory Shapefile*, Reston, Va. [Available at https://www.sciencebase.gov/catalog/item/56d692bde4b015c306f282ec.]
Uma, K. O., B. C. E. Egboka, and K. M. Onuoha (1989), New statistical grain-size method for evaluating the hydraulic conductivity of sandy aquifers, *J. Hydrol.*, *108*(1–4), 343–366, doi:10.1016/0022-1694(89)90293-X.
Van Kampen, N. G. (1992), *Stochastic Processes in Physics and Chemistry*, Elsevier, Amsterdam.
Vervier, P., J. Gibert, P. Marmonier, and M. J. Doleolivier (1992), A perspective on the permeability of the surface freshwater-groundwater ecotone, *J. North Am. Benthol. Soc.*, *11*(1), 93–102, doi:10.2307/1467886.
Ward, A. S. (2016), The evolution and state of interdisciplinary hyporheic research, *WIREs Water*, *3*(1), 83–103.
Ward, A. S., M. N. Gooseff, M. Fitzgerald, T. J. Voltz, and K. Singha (2014), Spatially distributed characterization of hyporheic solute transport during baseflow recession in a headwater mountain stream using electrical geophysical imaging, *J. Hydrol.*, *517*, 362–377.
Webster, J. R., and B. C. Patten (1979), Effects of watershed perturbation on stream potassium and calcium dynamics, *Ecol. Monogr.*, *49*(1), 51–72, doi:10.2307/1942572.
Withers, P. J. A., C. Neal, H. P. Jarvie, and D. G. Doody (2014), Agriculture and eutrophication: Where do we go from here?, *Sustainability*, *6*(9), 5853–5875, doi:10.3390/su6095853.
Worman, A., A. I. Packman, H. Johansson, and K. Jonsson (2002), Effect of flow-induced exchange in hyporheic zones on longitudinal transport of solutes in streams and rivers, *Water Resour. Res.*, *38*(1), doi:10.1029/2001WR000769.
Worman, A., A. I. Packman, L. Marklund, J. W. Harvey, and S. H. Stone (2007), Fractal topography and subsurface water flows from fluvial bedforms to the continental shield, *Geophys. Res. Lett.*, *34*, L07402, doi:10.1029/2007GL029426.
Zagni, A. F. E., and K. V. H. Smith (1976), Channel flow over permeable beds of graded spheres, *J. Hydraul. Div. Am. Soc. Civ. Eng.*, *102*(2), 207–222.
Zaramella, M., A. I. Packman, and A. Marion (2003), Application of the transient storage model to analyze advective hyporheic exchange with deep and shallow sediment beds, *Water Resour. Res.*, *39*(7), 1198, doi:10.1029/2002WR001344.
Zarnetske, J. P., M. N. Gooseff, W. B. Bowden, M. J. Greenwald, T. R. Brosten, J. H. Bradford, and J. P. Mcnamara (2008), Influence of morphology and permafrost dynamics on hyporheic exchange in arctic headwater streams under warming climate conditions, *Geophys. Res. Lett.*, *35*, L02501, doi:10.1029/2007GL032049.
Zarnetske, J. P., R. Haggerty, S. M. Wondzell, and M. A. Baker (2011a), Labile dissolved organic carbon supply limits hyporheic denitrification, *J. Geophys. Res.*, *116*, G04036, doi:10.1029/2011JG001730.
Zarnetske, J. P., R. Haggerty, S. M. Wondzell, and M. A. Baker (2011b), Dynamics of nitrate production and removal as a function of residence time in the hyporheic zone, *J. Geophys. Res.*, *116*, G01025, doi:10.1029/2010JG001356.
Zhou, D. H., and C. Mendoza (1993), Flow through porous bed of turbulent stream, *J. Eng. Mech.*, *119*(2), 365–383, doi:10.1061/(ASCE)0733-9399(1993)119:2(365).